Marine and Petroleum Geology 112 (2020) 104094

Contents lists available at ScienceDirect

Marine and Petroleum Geology

journal homepage: www.elsevier.com/locate/marpetgeo

Research paper

Estimation of deformation temperatures, flow stresses and strain rates from an intra-continental shear zone: The Main Boundary Thrust, NW Himalaya (Uttarakhand, India)

Narayan Bose[a], Soumyajit Mukherjee[b,*]

[a] Department of Geology and Geophysics, Indian Institute of Technology Kharagpur, Kharagpur, 721302, West Bengal, India
[b] Department of Earth Sciences, Indian Institute of Technology Bombay, Powai, Mumbai, 400 076, Maharashtra, India

A R T I C L E I N F O

Keywords:
Main boundary thrust
Thermometry
Piezometry
Strain rate
Flow stress
Laser Raman spectroscopy

A B S T R A C T

This work generates thermal and tectonic data from the mylonitized rocks of the Main Boundary Thrust (MBT). South and north to this major thrust, the Siwalik range and the Lesser Himalaya, respectively have been receiving a renewed interest amongst the petroleum geoscientists. Understanding temperature, flow stress and strain rates related to a major thrust is crucial in thermal-mechanical modelling of the terrains adjacent to it. Strongly sheared Proterozoic Chandpur phyllites and abundant syntectonic quartz veins occur along the MBT zone (one of the major foreland verging thrusts in the Himalayan orogen) near the Sahenshahi temple at Dehradun, Uttarakhand state, India. Microstructure analyses show intense ductile top-to-S shear in terms of S-C fabric and XRD analyses indicate presence of clays e.g., illite and clinochlore. These clays not only bear the signatures of the intense fluid activity, but also enhance the fault movement by reducing the mechanical strength of the fault zone rocks. Thermometry based on qualitative quartz grain boundary mobility (~300–550 °C) and quantitative Laser Raman Spectroscopy for carbonaceous materials (340–370 °C) reveal the maximum estimates of the deformation temperature and metamorphic temperature, respectively. The higher temperature microstructures can be found in lower temperature domains under the presence of fluids. Hence the quartz thermometry estimates a broader temperature range than the Raman thermometry. Previous works report that, the phyllites present at the base of a thrust sheet, experiences deformation at < 500 °C. The thermometric estimates in this study indicate a higher temperature at the base than that at further north known from previous studies, possibly by shear heating. A flow stress of ~6–49 MPa has been calculated from recrystallised quartz grain piezometry. This broad range of flow stress value indicates temporally variable tectonic stress responsible in the evolution of the MBT. Using these magnitudes, $\sim10^{-15}$-10^{-16} s^{-1} of strain rate has been estimated. Such a range can also indicate seismic cycles in the tectonically active Himalaya.

1. Introduction

In 1960s the Oil and Natural Gas Commission (ONGC) attempted hydrocarbon exploration in the Himalaya, a collisional orogen, which is also described as a fold-thrust-belt. A limited success was achieved mainly in terms of gas discovery from the Siwalik range, especially from Himachal Pradesh (review in Mishra and Mukhopadhyay, 2012). Notwithstanding, ONGC (e.g., Rao, 1986) and other research bodies (e.g., Mukherjee and Chakrabarti, 1996) continued independent petroleum geological studies in other sectors of the Himalaya.

The Eocene limestones that crop out near the Main Boundary Thrust (MBT) and also from the Lesser Himalayan sequence (LHS) have given few oil and gas shows (Acharyya and Ray, 1982). Based on palaeontological studies, Ediacara in particular, Tewari (2012) predicts the presence of hydrocarbon source rock from the Neo-Proterozoic terrain of the LHS in the Garhwal sector. Interestingly, Neoproterozoic-Cambrian hydrocarbon reserves started receiving attention amongst the geoscientists worldwide, a few study areas exist in western India itself e.g., the Bikaner Nagaur basin (Bhat et al., 2012; Ojha, 2012). Within the Himalaya, the Proterozoic rocks of the Jammu region (NW Himalaya, India) is presently under study for hydrocarbon (Hakhoo et al., 2016). The line of comparison between the western Indian basin and the Lesser Himalayan region is the age of the rocks. The detail tectonic set up however differ. The reason of comparison is that it will be unwise to think that the very old rock in the Lesser Himalaya cannot be petroliferous.

* Corresponding author.
E-mail addresses: soumyajitm@gmail.com, smukherjee@iitb.ac.in (S. Mukherjee).

https://doi.org/10.1016/j.marpetgeo.2019.104094
Received 26 May 2019; Received in revised form 1 October 2019; Accepted 14 October 2019
Available online 26 October 2019
0264-8172/

As the easy to discover oil fields get depleted, the oil industry has been revising its plan to make a more intense study on the Himalaya. For example, ONGC has been targeting the Krol unit of rocks from the LHS that lies close to the MBT (Bhattacharya, Internet Reference). This is because previous workers have categorized the Krol and Tal units of the LHS as a potential reservoir of moderate quality (reviewed in table 1 of Mishra and Mukhopadhyay, 2012). Besides those two stratigraphic units of the LHS, the Blaini unit has also been considered to be important (Craig et al., 2018). While a detail sequence stratigraphic study have been undertaken by Jiang et al. (2002) in these areas, recent detail structural studies is missing, except Bose and Mukherjee (2019a) which was but on a different perspective.

Regional anticlines within the Siwalik range, the southernmost unit of the Himalaya, exist adjacent to the MBT, e.g., the Santaugarh anticline (a fault propagation fold: Thakur et al., 2007a, b) in the Garhwal Himalaya, where a reconnaissance survey can be undertaken. Since structural geology within fold thrust belts fundamentally controls the spatial occurrence of the hydrocarbon reserves (Cooper, 2007), this work aims to deduce fundamental thermal and tectonic parameters from the MBT region that will be useful in future thermal-mechanical modelling of the adjoining terrains.

Quantification of deformation temperature (Cavalcante et al., 2018; Mazza et al., 2018), flow stress (Christie and Ord, 1980; Gueydan et al., 2005) and strain rate (Handy, 1994; Sassier et al., 2009) are prerequisite to understand the deformation mechanisms of rocks. This would enable interpretation of tectonics of the terrain under study. Factors such as fluid-pressure, grain-size and composition greatly influence the development of shear zones (e.g., Schmid, 1982; Arch et al., 1988; Wojtal and Mitra, 1988) and their impacts should be understood properly in studying shear zones (e.g., Law, 1990; Newman and Mitra, 1994; Bhattacharyya and Mitra, 2011, 2014; Bose et al., 2018). At one side, research groups (e.g., Kali et al., 2010; Long et al., 2011; Yakymchuk and Godin, 2012; Law et al., 2013) have deduced the temperature a shear zone can attain. On the other hand, other research communities have modelled the shear-related heating (e.g., Nabelek et al., 2001; Whittington et al., 2009; Mulchrone and Mukherjee, 2016; Mukherjee, 2017a). With the help of such thermometric studies, at some point geoscientists might predict shear zone temperatures (e.g., Wolfowicz, 2012) from models. Then they would be able to check how far they match with the estimated value from the natural deformations. Closer the match, better will be the understanding of the shear zone kinematics. Factors like temperature, flow stress and strain rate provide the details of the deformation process. These factors also control the switch between the elastic and plastic deformational regimes, which link with the seismic-aseismic cycles (e.g., Handy, 1989; Kruhl et al., 2007; Rogowitz et al., 2014). Earthquake frequencies are very closely related to strain rates (Shen et al., 2007).

Following this trend, this work uses a few widely used techniques (e.g., Goscinak, 2014; Farrell, 2017) to estimate the deformation temperature, flow stress and strain rate.

2. Geology and tectonics

Around 11 Ma years back (Meigs et al., 1995), the MBT zone placed the hangingwall block of the Proterozoic Lesser Himalayan Sequence (LHS) at N/NE over the footwall of the Cenozoic Sub-Himalayan Siwalik Supergroup at S/SW (review in Yin, 2006) (Fig. 1a–c). Some authors consider the MBT as a basement thrust (Raina, 1978). The MBT usually dips 30–50° but at few places is sub-vertical (Thakur et al., 2007a, b). The LHS, situated between the MBT and the Main Central Thrust (MCT), is subdivided into two tectono-stratigraphic units – the northern Paleoproterozoic Inner LHS, and the southern Neoproterozoic-Cambrian Outer LHS (lithotectonic units of the Garhwal Lesser Himalaya in Repository Table 1). These are separated by a ~ NE-SW trending Tons thrust in the Garhwal Himalaya (Célérier et al., 2009a,b and references therein). The LHS in the Garhwal Himalaya (Bose and Mukherjee, 2019a) and elsewhere (Bose and Mukherjee, 2019b) underwent top-to-N/NE back-thrusting of unconstrained timing. By GPS study in the Kumaun Lesser Himalaya, Ponraj et al. (2010) deduce 15 mm yr^{-1} present day convergence rate. The active nature of MBT is also reflected through various other signatures, such as landslides (Panikkar and Subramanyan, 1996; Joshi et al., 2011), semsmicity (Pathak et al., 2015) and radon emissions (0.04 ± 0.01 to 0.58 ± 0.04 pCi/ml) near Dehradun, Uttarakhand (Ramola et al., 1988). Since Ramola et al. (1988) find radon emission from the MBT fault zone itself, they do not faour any reason for this emission other than the MBT activity. However, in other parts of the Garhwal Himalaya, the MBT is presently inactive (Jayangondaperumal et al., 2018).

This study was conducted in the litho-units of the MBT hangingwall rocks, i.e., the Chandpur Formation of the Outer LHS in the Garhwal Himalaya. The Chandpur Formation mainly comprises of shales, phyllites, siltstones and sandstones. The mineral assemblage (e.g., epidote micas, such as chloritized recrystallised biotite) suggests a greenschist facies metamorphism (Islam et al., 2011). Following the U-Pb dating method, an age of 8239.5 Ma was deduced from the magmatic zircons of the Lesser Himalayan Chor Granitoids (Singh et al., 2002). The black Chandpur phyllites expose along the MBT zone near Dehradun where the Mussourie hills start. Here, the MBT trends NW-SE. Based on the Raman Spectroscopy of Carbonaceous Material (RCSM), Célérier et al. (2009a,b) calculate < 330 °C temperature for the various low-grade meta-sedimentary rocks from the Kumaun and the Garhwal Lesser Himalaya. Mineralization of Pb, Zn, U, gypsum and barite have been reported north to the MBT, within the LHS (review in Ghose, 2006).

3. Methods

3.1. Sampling

Fieldwork was carried out around the Sahenshahi Ashram (N 30° 24′19.4′′, E 78° 05′42.9′′) Dehradun, close to the MBT. Here the MBT zone has thrust the black pelitic rocks of Chandpur Formation over the Siwalik conglomerates (Fig. 2a). Intensely top-to-S sheared black Chandpur phyllites along with abundant quartz veins crop out along the MBT zone that trend N-S (Fig. 2b–d). Two phyllite and two quartz-vein samples were collected from this spot. Quartz vein samples were collected from a single vein.

Naturally deformed samples were collected for these purposes from the low-grade outer Lesser Himalayan Sequence, exposed along the Main Boundary Thrust (MBT) zone near Dehradun, Uttarakhand, India, western Himalaya. The data generated for the MBT in this work would act in better understanding of thermal and dynamic behaviour of the natural shear zone: the MBT.

3.2. Microstructures & clay mineralogy/XRD analysis

Thin-sections of the phyllite and the quartz vein were prepared that orient perpendicular to the N-dipping main foliation and parallel to the dip direction of those foliation planes. For clay-separated XRD analyses, the samples were powdered (< 75 µm) at first. This was followed by the usual processing through decantation and centrifuge to extract clays. The air-dried samples were studied in the PANalytical Empyrean (PANalytical B.V., Almelo, The Netherlands) set up at the Department of Earth Sciences, IIT Bombay. Final results were obtained through the HighScore Plus software v. 4.6a (Degen et al., 2014) and the Inorganic Crystal Structure Database. The fundamentals of the XRD analyses can be found elsewhere (e.g., Moore and Reynolds 1989; Poppe et al., 2001).

3.3. Quartz deformation thermometry

Thin-sections made from samples of Chandpur phyllites as well as

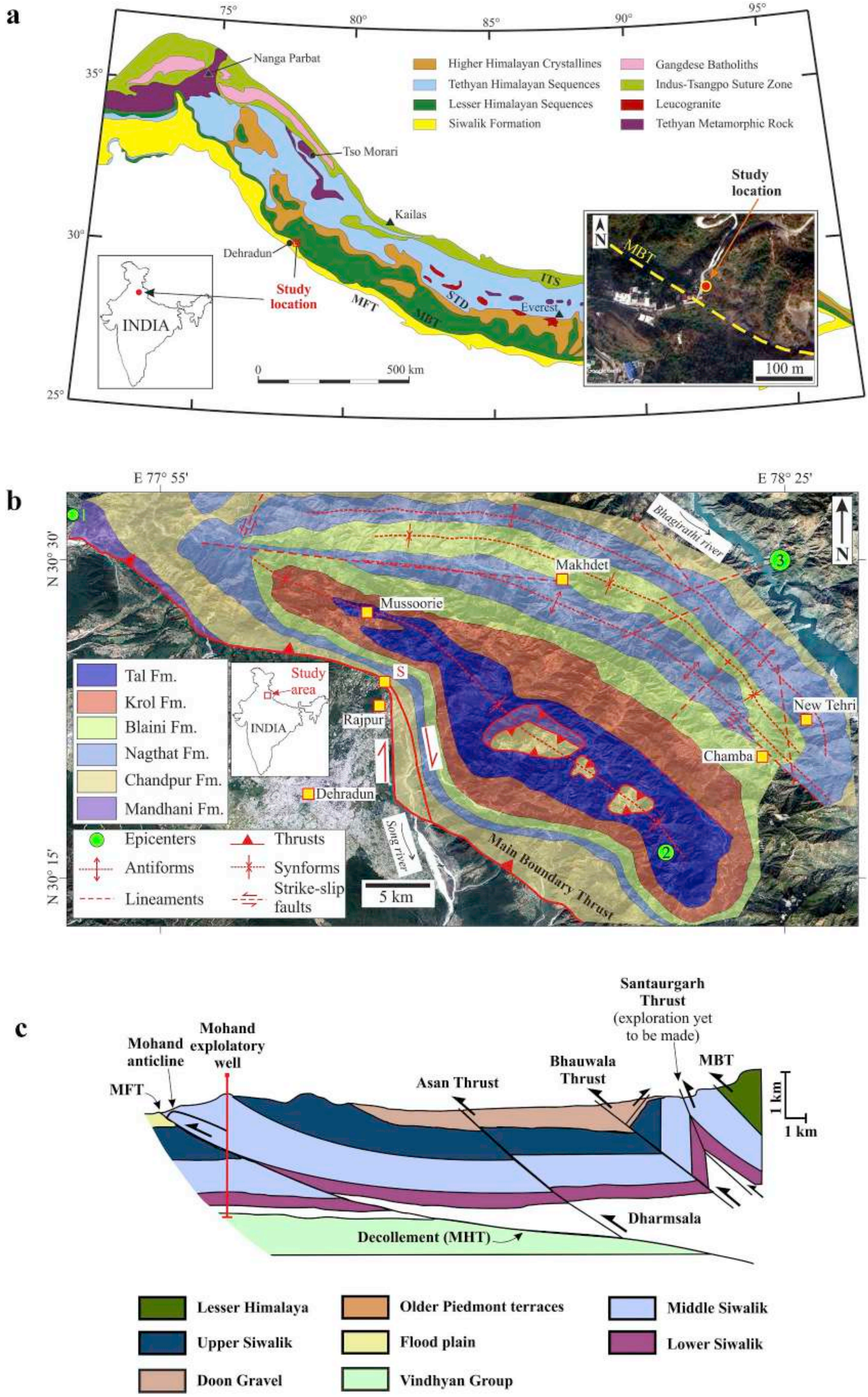

(caption on next page)

Fig. 1. a. Simplified geo-tectonic divisions of the Himalaya (reproduced from Fig. 1 of Mukherjee et al., 2015). Study location plotted. **b.** Geological map of the Garhwal Inner Lesser Himalaya (redrawn after Fig. 1 of Jayangondaperumal and Dubey, 2001), superposed on the Google Earth satellite imagery. S: study location, Sahensahi Ashram (N 30° 24′19.4′′, E 78° 05′42.9′′). Data for the earthquake epicentres is presented in the following table. Data source: United States Geological Survey website (https://earthquake.usgs.gov/earthquakes/search/), accessed on 27-May-2019.

Sl. No.	Date	Latitude (N)	Longitude (E)	Depth (km)	Magnitude (Mw)
1	02-Jan.-1997	30.536	77.844	33	3.5
2	03-May-2010	30.27	78.314	13.5	4
3	03-May-1984	30.5	78.404	33	4.5

c. Geological cross-section through the Garhwal Sub-Himalaya. Reproduced from Fig. 2 of Dutta et al. (2019), originally drawn by Thakur and Pandey (2004).

quartz veins were studied for micro-structural and thermometric analyses. Experimental studies (Rutter, 1974; Tullis and Yund, 1985; Stipp et al., 2002; review in Passchier and Trouw, 2005) show that quartz develops characteristic microstructures. These microstructures are governed dominantly by increasing temperature. Repository Table 2 summarises such observations of previous workers. Other factors such as pressure, strain rate, presence of water also play roles. For example, the higher temperature microstructures can be present in the lower temperature condition, if either the strain rate is low or the water content is high (Griggs, 1967; Law, 2014; Stünitz et al., 2017).

3.4. *Thermometric study using laser Raman Spectroscopy for carbonaceous materials (LRSCM)*

See Appendix-1 for a glimpse of fundamental principles of LRSCM. Beyssac et al. (2002) applies the LRSCM technique on a variety of rocks (black shale, mica schist, marble, anthracite, granulite) collected from Schistes Lustre's unit, W. Alps and from the Sanbagawa metamorphic belt, Japan. They come up with the following empirical equation to estimate the peak metamorphic temperature, which has been widely followed by the subsequent workers (e.g., Nagy and Toth, 2012):

$$T\,°C = -445 \times R2 + 641 \tag{1}$$

Here, R2 = D1/ (G + D1 + D2) peak area under the curve ratio (Repository Fig. 1). With an error limit of ± 50 °C, eqn. (1) estimates the deformation temperature within the range 330–650 °C. The equation does not depend on the metamorphic grade of the rock nor the source of the carbonaceous materials. Eqn (1) was modified in few cases by researchers but even then nearly the same results were obtained (Nagy and Toth, 2012).

Rahl et al.'s (2005) LRSCM studies on low-grade (< 300 °C) metasedimentary rock samples collected from Crete (Greece), South Island (New Zealand) and Olympics Mountains (USA) lead to formulate another empirical equation using the R1 and the R2 ratios. The R1 ratio is given by D1/G peak height (intensity) ratio (Repository Fig. 1). The formula is:

$$T\,°C = 737.3 + 320.9 \times R1 - 1067 \times R2 - 80.638 \times R1^2 \tag{2}$$

This formula has been tested successfully by those authors, for 100–700 °C with an error of ± 50 °C.

Fig. 2. (a) MBT zone characterized by extremely deformed black pelites on hanging wall block. Conglomerates crop out at the footwall block. **(b–d)** Nature of black pelitic rock along with quartz veins exposed at MBT zone. Studied samples were collected from these exposures. **(d)** The angle between Y- and P-planes is 41°.

Eqns. (1) and (2) have been widely applied on a variety of rock types and tectonic situations (e.g., Kouketsu et al., 2014; Hu et al., 2015). Petrographic thin-sections are feasible since they allow the in-situ measurements of the Laser Raman spectra, the relationship between carbonaceous material (CM) and mineral matrix can be observed. Due to its anisotropic structure (i.e., deformation varies with crystallographic orientation), orientation of the CM affects the generated spectra. The use of thin sections also aids in the removal of the laser-generated heat by the mineral matrix (Beysssac et al., 2002). According to Beyssac et al. (2003), the CM being opaque, the laser can penetrate ~ 10–100 nm of the CM. This thin zone of CM can get affected during sample preparation procedure. To overcome this, a minimum polishing was done on the thin-sections and a CM grain lying beneath a transparent grain (e.g., quartz) was preferred during the LRSCM. Again the structural-order of the CM structure, hence the obtained results, depends on the precursor and metamorphic conditions (Quirico et al., 2009). This bias does not influence the results of this study as samples were taken from a single spot location.

The LRSCM was performed through a Laser Raman WD Almega XR spectrometer (manufactured by Thermo-Nicolet) equipped with a confocal optics and CCD detectors. A 50× objective with 25 μm pinhole was used to focus the 12.5 Mw (50%) 532 Ar green laser beams on the sample and the acquisition time was 30 s for each of the total 18 sample points belonging to 4 thin-sections of the black phyllonitic rock. After the acquisition of spectra, baseline correction and curve fitting were done using the *software OriginPro (v. 8, Origin Lab, 2007)* and the data were used for further calculations.

3.5. Flow stress estimation by piezometry using recrystallised quartz grain size

Tectonic stresses result in creep of rocks causing a displacement of the dislocations that increases crystal defects. During creep, the dislocations in a grain accumulate and eventually become the subgrain boundary. The number of such subgrain boundaries increase with increasing flow stress. Hence the increase in flow stress (measured as differential stress) reduces sizes of the individual subgrains (White, 1977; Twiss and Moores, 2007). When a subgrain attains a different crystallographic orientation than its parent grain, it becomes a recrystallised grain. The recrystallised grain size, which is a better palaeopiezometric tool than the sub-grain size/dislocation density (Ord and Christie, 1984), can be correlated with the flow stress using the following equation (Ludwigson, 1971):

$$\mathrm{Yf} = \mathrm{K}e^{n} \tag{3}$$

Yf: flow stress (in MPa), equivalent to deviatoric stress; K: strength coefficient (in MPa), a material property denoted by a constant value; e: strain (unitless); n: strain hardening exponent (unitless), a material constant. A uniform plastic behaviour of the material has been presumed in Eqn. (3). This equation works for metals and alloys. The magnitude of K for quartz is not known, to the knowledge of the authors.

Following this relationship, Twiss (1977) propose the following theoretical and global piezometer:

$$\sigma = \mathrm{B}d^{-0.68} \tag{4}$$

Here σ: differential stress in MPa; B: 5.5 MPa μm^{-1} for quartz; d: recrystallised grain size given as the diameter of circle with equal area of the grain. The parameter B in Eqn. (4) is a constant in the empirical formula.

Stipp and Tullis (2003) propose another empirical piezometer based on the axial compression experiments on Black hill quartzite carried out in a Griggs apparatus using molten salt cell:

$$D = 10^{3.56\pm0.27} \times \sigma^{-1.26\pm0.13} \tag{5}$$

Here D: recrystallised grain size in μm, given as the diameter of circle with equal area; σ: flow stress. For a large number of grains, it is better to use the median value of the grain size distribution, than the mean value (Ranalli, 1984). Stipp and Tullis (2003) check the applicability of this piezometer for dynamically crystallised rocks with 3–45 μm grain size.

However, Stipp et al. (2010) apply this piezometer on quartz mylonites with 3 μm - 3 mm grain-sizes. They plotted the BLG-SGR and SGR-GBM domain boundaries at ~35 μm and 120 μm, respectively. This scheme has been globally used by the subsequent workers (e.g. Hunter et al., 2018) as well as in the current study. Finding a more accurate flow law is underway (Lu and Jiang, 2019). Flow laws derived from lab experiments well suits naturally deformed mylonites (Lu and Jiang, 2019). On both the mono-mineralic and polymineralic rocks, the flow laws work (Ji and Xia, 2002). Previous workers also tried to formulate an equation for strain-rate calculations (e.g. Poirier, 1985; Tsenn and Carter, 1987). However, Hirth et al. (2001) provided a more accurate empirical equation to estimate the strain-rate of natural samples. Hence, the later equation has been used in the current study. This is explained in detail in the Appendix-2.

Although not considered in this work, other factors like temperature and presence of fluid influence this process. While experimenting on the olivine aggregates with low water content, Drury (2005) presumes the recrystallised grain size to be independent of temperature. However, during lab experiments with polycrystalline halites, ter Heege et al. (2005) conclude that the temperature plays a significant role in palaeostress estimation and the temperature independent piezometers underestimate the flow stress. Lab experiments on quartzites by Stipp et al. (2006) do not find any influence of water on the flow stress estimations. However, these piezometers (eqns. (4) and (5)) have been widely used to study natural shear zones (e.g. Austin, 2011; Singleton et al., 2018), including phyllonites (e.g. Krabbendam et al., 2003; Menant et al., 2018).

3.6. How to estimate strain rate

There are different types of structural analysis to determine stress-strain relationships and associated deformation features in field. Mohr diagram (e.g., Mukherjee et al., 2019) can be one of them. The strain rate indicates the rate at which the material deforms. The parameter also gives an idea about the rate of strain accumulation (Prescott et al., 1979; Fossen, 2016).

There is a power law relation amongst flow stress, deformation temperature and strain rate for a quartz vein deforming through dislocation creep. Studying the quartzite samples from the Ruby Gap duplex, Australia, Hirth et al. (2001) present the following empirical equation to estimate strain rate in natural samples:

$$\varepsilon^{\cdot} = A \times f_{H_2O}^{m} \times \sigma^{n} \times e^{(-Q/RT)} \tag{6}$$

Here

$\varepsilon^{\cdot\cdot}$: strain rate (per second); A: a material parameter = 10–11.2 MPa-n s^{-1} (for quartz); f_{H2O}: water fugacity; m: water fugacity exponent = 1; σ: flow stress; n: stress exponent = 4; Q: activation energy = 135 kJ mol^{-1}; R: molar gas constant = 8.3145 J/mol-K; T: deformation temperature in Kelvin scale. Due to its very low impact on $\varepsilon^{\cdot\cdot}$ (Stipp, per. comm.; Francsis, 2012), f_{H2O} not measured in the present study is justified. Eqn. (6) has been widely used to deduce strain rates (e.g., Boutonnet et al., 2013). See Appendix-3: Table- 1 for detail. Modification of the constituent terms in eqn (6) and its applicability on naturally deformed quartz bearing samples makes the equation the best choice in the current study. Mazzotti and Gueydan (2018) use this equation to model crust and mantle rocks. Samples of quartz veins are used in this study for strain-rate estimation for the MBT-related shear. While conducting experimental studies on wet quartzite, Tokle et al. (2019) utilize the dynamic recrystallised grains for stress estimation. Besides finding the similarities between natural and experimental deformation patterns, they also suggested two flow laws with different stress exponents: n ≈ 4 and 3 for lower and higher stresses, respectively.

Takahashi et al (1998) provide the following empirical formula to calculate strain rate:

$$D = \phi \log\dot{\varepsilon} + \frac{\rho}{T} + 1.08 \tag{7}$$

Here, D = fractal dimension = slope of the least-square linear fit in the diameter-perimeter log-log graph of the grains, $\phi = 9.34 * 10^{-2}$ $[\log(s^{-1})]^{-1}$, $\dot{\varepsilon}$ = strain rate, $\rho = 6.44 * 10^{2}$ K, T = temperature (in K). However, Mamtani and Greiling (2010) report that this method is not useful to calculate strain rate at high temperatures. Therefore, eqn (7) has not been used to calculate the strain rates in this study. The strain rate in a simple shear zone depends on the average slip rate and width of the strain accumulation zone (Boncio, 2008). Again, being a single spot study, this bias does not influence our results.

4. Results

4.1. Microstructural observations and clay minerals

Microstructural observations from phyllite (Figs. 3 and 4) show several deformation features, e.g.: *(i)* ductile shear (Fig. 3a and b) and brittle shear (Fig. 3d); *(ii)* contractional (Fig. 3a) and extensional features (Fig. 3a,c); *(iii)* brittle (Fig. 3c) and ductile (Fig. 4a,d) behaviour of quartz grains etc. Clay-separated XRD analyses indicate the presence of clinochlore (Mg-rich chlorite) and illite (Fig. 5).

4.2. Quartz deformation thermometry

The sheared quartz veins were studied for this part. The quartz grain boundary mobility features (Repository Table 2; Figs. 6 and 7) represent approximately the following deformation temperatures (Hirth and Tullis, 1992; Stipp and Tullis, 2003): *(i)* The fragmentation induced grain size reduction (Fig. 6a) and the intra- and inter granular fractures (Fig. 6b,d) indicate cataclasis (< 300 °C). Note that during cataclastic flow, intragranular fractures can also generate by minor plastic deformation (Evans, 1990); *(ii)* bulging in grain boundary (Fig. 6b), strain lamellae (Fig. 6c), sweeping extinction (Fig. 6d) and neocrystallisation along grain boundary (Fig. 7a and b) connote a Bulging Recrystallisation (BLG; 300–400 °C); and finally *(iii)* static recrystallisation indicated by polygonal quartz grains (Fig. 7c) and elongated quartz grains (Fig. 7d) imply a Subgrain Rotation (SGR; 400–500 °C). Note that samples from which Figs. 3 and 4 come have not been used in thermometric study here.

The deformation in the studied MBT zone started when it was in the ductile regime. It is presently exposed at the surface possibly due to slip along the MBT and subsequent erosions. Hence, the higher temperature older textures in the MBT zone rocks are likely to be overprinted by younger lower temperature deformation features (e.g. Wojtal and Mitra, 1988; Srivastava and Mitra, 1996; Bhattacharyya and Mitra, 2014). In this study, the lower temperature (cataclastic flow; < 300 °C) features discussed above (Section 4.2) indicate that during the later successive deformations, the temperature of deformation fell down to < 300 °C. According to Passchier and Trouw (2005), during deformation, structures overprint first by higher temperature signatures (up to the peak metamorphic condition). This is followed by the lower temperature features. They also suggest that the features preserved in thin-sections get 'frozen in' just before the temperature as well as strain rate go below a critical value during the final stages of the competing processes. In the studied thin sections, such features are indicated by the co-existence of elastic-plastic signatures (Figs. 6 and 7). As a result, signatures of deformations at lower and higher temperatures are present in the studied thin sections. However, presence of clays and pressure solutions indicate intense fluid activity. This might have induced hydrolytic weakening (Griggs, 1967; Snoke, 1998) of the studied rock. Hence, the quantifications made here are the maximum estimates.

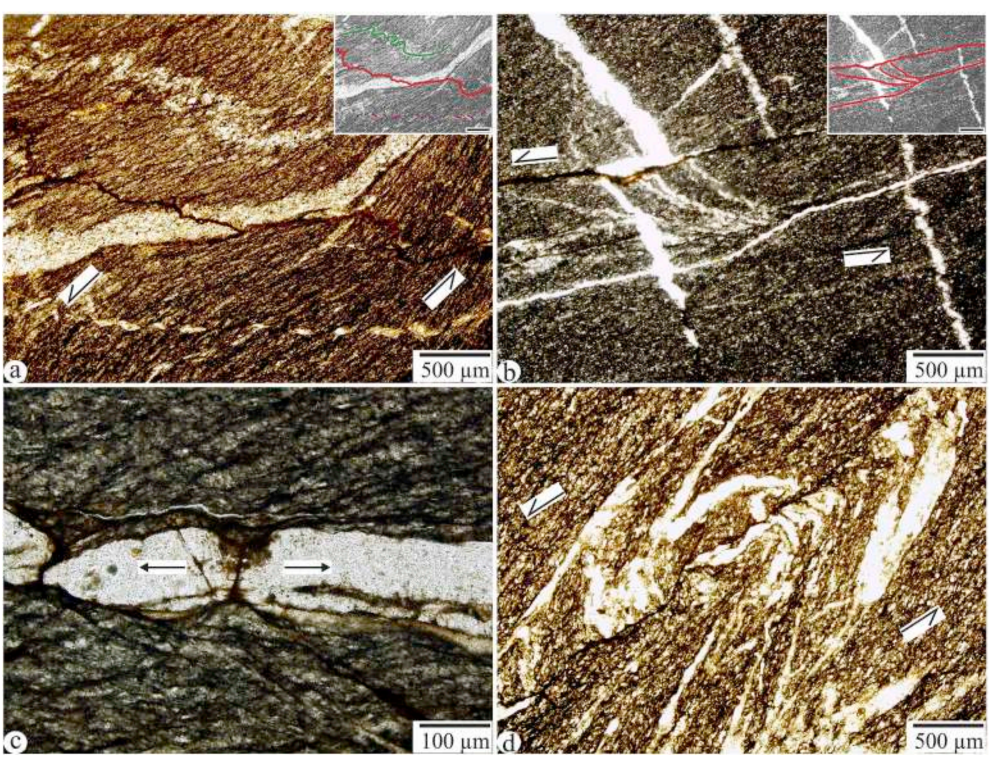

Fig. 3. **(a)** Quartz veins (marked as 1, 2, 3) show three types of deformations. The upper one (1) is folded and represents a contraction. The middle vein (2) is more or less parallel with the foliation in the matrix. Here a step fracture (red broken ellipse) indicates an anti-clockwise (top-to-SW) brittle shear. The lower vein (3) shows shear boudins, which indicate an extension in a brittle regime. Black host rock with quartz veins, plane polarised light. **(b)** The central (red broken ellipse)S-C fabric gives an anti-clockwise (top-to-SW) shear. Transgranular truncation of fractures (high angle with the S-C zone) and their folding are observed. Black country rock, plane polarised light. **(c)** Pinching in quartz vein resulting fracture in quartz vein & neck folds of foliations in host rock were observed. The pattern of foliations in one side of the host rock is opposite to the pattern in other side. Black rock with quartz vein, plane polarised light. **(d)** Quartz veins truncate a brittle shear fracture plane made up of Riedel shears (Passchier and Trouw, 2005 and references therein). A rootless fold of quartz, bending of quartz veins near the fracture plane is noticeable. Black rock, plane polarised light. (For interpretation of the references to colour in this figure legend, the reader is referred to the Web version of this article.)

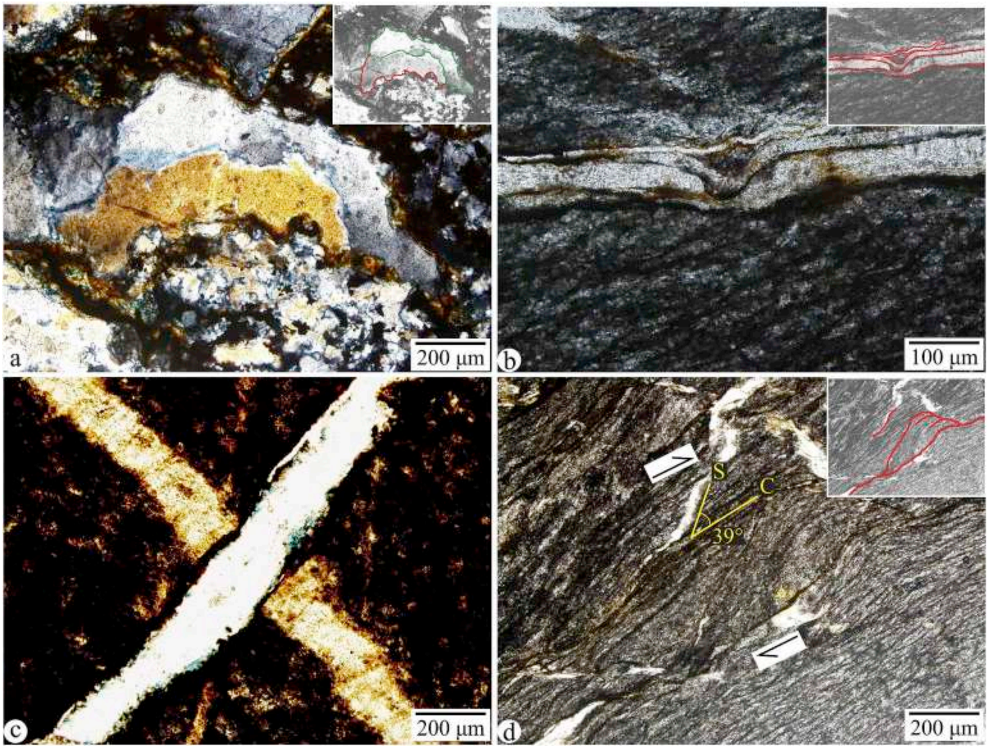

Fig. 4. (a) One quartz grain overrides the other, surrounded by clay minerals (brownish yellow - black). Elongated grains, bulged boundaries with triple junction and polygonal contacts are noticed. Quartz vein, crossed polarized light. **(b)** Extension related thinning in the lower (thickest) quartz vein and neck fold in the middle vein. Whereas, the upper (thinnest) vein is folded. Black host rock with quartz vein, plane polarised light. **(c)** Younger quartz vein cuts across the older one. Black host rock with quartz vein, plane polarised light. **(d)** Pattern of shear foliations in black pelitic rock. Clockwise shear is shown by S-C fabrics and en-echelon stacks. Here, the angle between S- and C- fabric is 39°. Black pelitic rock, plane polarised light. (For interpretation of the references to colour in this figure legend, the reader is referred to the Web version of this article.)

4.3. Laser Raman Spectroscopy for carbonaceous materials (LRSCM)

After the decomposition of the laser Raman spectra of the carbonaceous materials present in the MBT zone Chandpur phyllites (Repository Figs. 1 and 2), parameters such as the band position, the peak width, the peak height and the area under the peak were calculated to determine the temperature of deformation (Figs. 8 and 9). The peak metamorphic temperature values calculated using eqn. (1) ranges 307–456 °C, with 374 °C as the mean value. Similarly, eqn. (2) gives a data set between 200 and 500 °C yielding a mean value of ~356 °C. Both the estimates involve ± 50 °C error.

4.4. Piezometry

Areas of recrystallised quartz grains were measured from the photomicrographs of two thin-sections of quartz veins present in the

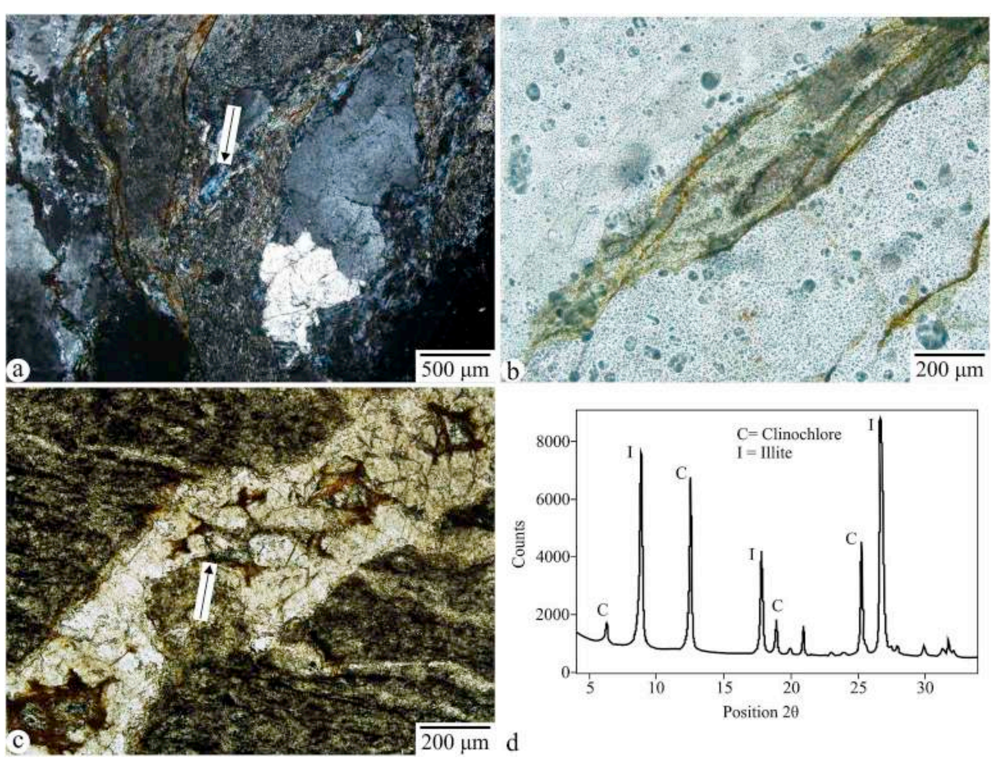

Fig. 5. (a–c) Clays present in the sample(examples indicated by arrows). **(d)** Result of clay-separated XRD analyses.

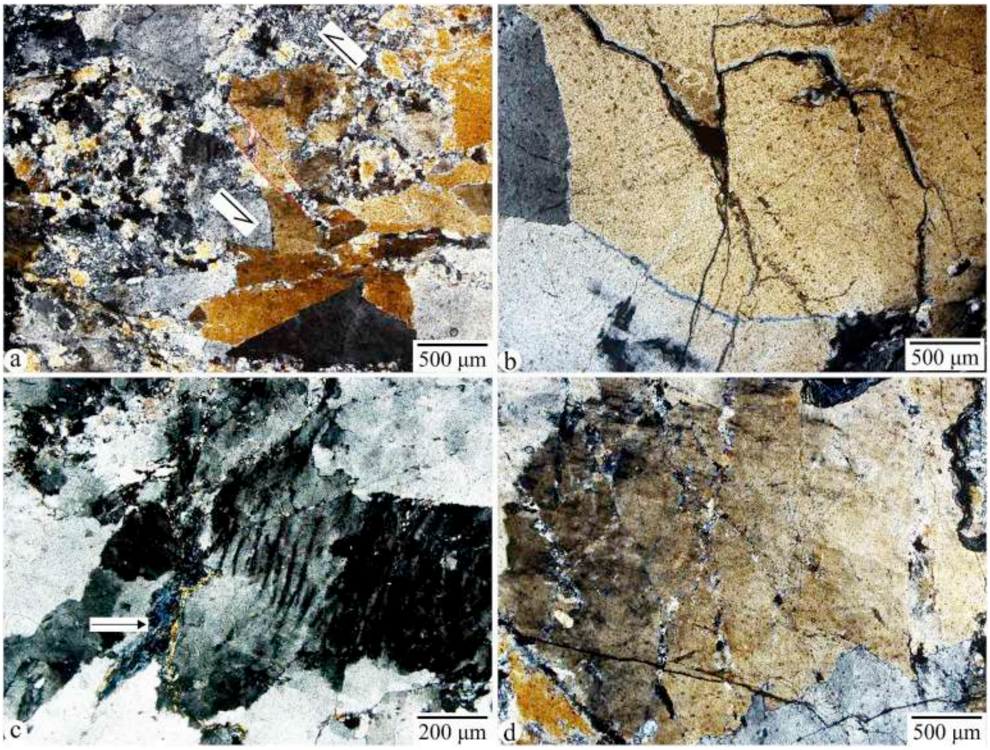

Fig. 6. (a) Breakage by brittle fracture, zone of small new grains, angular fragments ofquartz etc. indicate a cataclastic flow condition (< 300 °C). Micro-faulting of the central yellow grain is noticeable. Quartz vein, plane polarised light. **(b)** Parallel sets of fractures show abating relation with a central fracture plane. Quartz vein, plane polarised light, width of view~ 3.5 mm. Various types of brittle fractures indicate that the quartz vein deformed in brittle regime at a temperature < 300 °C. Various types of brittle fractures indicate that the quartz vein deformed in brittle regime at a temperature < 300 °C. Bulging at triple junction and deformation lamellae (top black grain) indicate a bulging recrystallisation condition (300–400 °C). Formation of very fine new grains along boundaries is identified by light grey colour. Although highly sutured boundary indicates that the deformation took place at a higher temperature (> 500 °C). Quartz vein, plane polarised light. **(c)** Strain induced deformation lamellae, deformation banding, sweeping extinction along with sutured and serrated grain boundaries indicate bulging recrystallisation (300–400 °C). Quartz vein, plane polarised light. Arrow indicates clays. **(d)** Inter-fingered grain boundary, wavy extinction, recrystallisation along subgrain boundaries indicates BLG condition (300–400 °C). Quartz vein, plane polarised light. (For interpretation of the references to colour in this figure legend, the reader is referred to the Web version of this article.)

phyllitic rock of the MBT zone. The software *'J-microvision'* (v. 1.2.5 by Nicolas Roduit, 2007) was used. Total 200 grains of recrystallised quartz were measured from all the thin sections (e.g., Fig. 7c). According to the method followed by Stipp et al. (2010), the grouping of the grains were done based on their grain diameters, i.e. < 40 μm for Bulging Recrystallisation (BLG), 40–120 μm for Sub-grain Rotation (SGR), and > 120 μm for Grain Boundary Migration (GBM). Amongst those 154 grains come under the SGR deformation zone, 45 grains

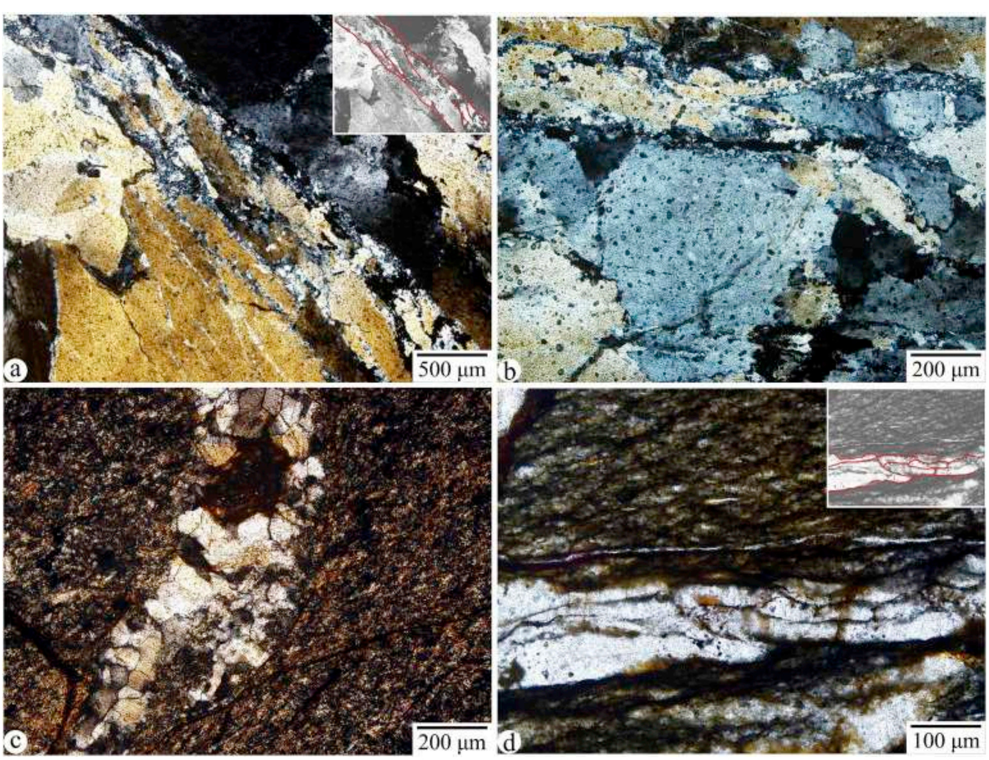

Fig. 7. (a) Strain induced dynamic recrystallisation in quartz vein. Larger quartz grains. With undulose extinction form elongated subgrains. Recrystallisation (or, subgrain to recrystallisation transition) around elongated subgrains indicates BLG as the dominating recrystallising process (300–400 °C). Intra-granular microcrack (bottom left), aligned trails of inclusion (right centre) are also noticed as these indicate deformation at lower temperature (< 300 °C). Quartz vein, plane polarised light. (b) Elongated subgrains of quartz (central and upper part) along with very small recrystallised grains (abundant in the top right segment) surrounding them indicate a BLG to SGR transitional condition (~400 °C). Whereas recrystallisation along grain boundaries, sutured/bulged grain boundaries in porphyroclasts indicate BLG (300–400 °C). A parallel trail of inclusions in the central grain indicates healing of micro-cracks at lower temperature (< 300 °C). Quartz vein, plane polarised light. (c) Straightening of boundary and polygonisation of recrystallised quartz grains indicate abrupt recovery and static recrystallisation in a strain free condition (400–500 °C). It is also evident from the random orientation in the grains. Minor bending in some grain boundaries may be due to incomplete recovery or bulging recrystallisation at lower temperature (300–400 °C) during later deformational phases. Black country rock with quartz vein, crossed polarized light. (d) Elongated quartz grains and bent grain boundaries indicate ductile deformation of the quartz grains These features along with brittle step-fractures (left) suggest a ductile-brittle phase. Black host rock with quartz vein, plane polarised light.

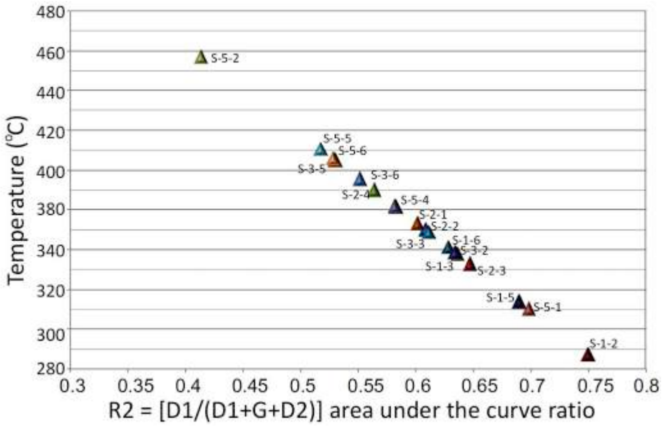

Fig. 8. Temperature calculated from the equation given by Beyssac et al. (2002).

belong to GBM recrystallisation, and only a single grain is of BLG recrystallisation (Fig. 11). The data (Repository Table 3) related to the area of the grains, diameter of equal area circles, and flow stresses (Fig. 10) have been calculated using both eqns. (4) and (5).

Flow stress values calculated according eqn. (4) show a maximum frequency in the 25–30 μm domain (55 values, 27.5% of total population). Whereas, the mean flow stress values calculated as per eqn. (5) show maximum frequency in the 15–20 μm domain (68 values, 34.0% of total population).

4.5. Strain rate estimation

The deformed quartz veins present in the MBT zone phyllite has been used here. A flow stress of 10.68–49.18 MPa was calculated from the given data set using eqn. (4). On the other hand, eqn. (5) gives 6.04 ± 1.05 to 35.88 ± 4.45 MPa for the same data set. From these values, a strain rate of 10^{-15} - 10^{-16} s^{-1} has been calculated (Table 1) using Eqn. (6).

5. Discussions

5.1. Veins

Synkinematic quartz veins, generally present at the base of the thrust sheet, bears the signatures of the corresponding fault activity (e.g. Coli and Sani, 1990; Henderson and McCaig, 1996; Cox, 1998; Blenkinsop, 2008; Wiltschko et al., 2009) and indicate elevated pore-fluid pressure (e.g. Boulton et al., 2009). As the synkinematic quartz veins bear the signatures of younger dynamic recrystalliastion deformations, these veins act as a very reliable tool to estimate the temperature, flow stress and strain rate related to the deformation phases (Haertel et al., 2013). Similarly, in the studied case the abundance of veins restricted at the base of the footwall block suggests their synkinematic nature. Additionally, the shear senses shown by the veins (Fig. 2c and d) matches with the foreland-vergent top-to-S shear sense of the MBT deduced from other kinematic indicators in the field in this work, and also by other researchers from different Himalayan sections (Yin, 2006), indicating that these veins are certainly not pre-Himalayan.

Further, nobody has reported conclusively any pre-Himalayan deformation from the MBT zone or from such regional main thrust zones from the Himalaya. The pre-/eo-Himalayan signatures such as angular unconformity, SW-verging folds in mega-scale, rootless tight to isoclinal folds with metamorphic banding along the axial plane foliation, sandstone dykes etc. (Garzanti et al., 1995 from Spiti, NW Himalaya; Wiesmayr and Grasemann, 2002 from NW Tethyan Himalaya; Jain et al., 2002 from the western Himalaya; Draganits et al., 2005 from Pin Valley, NW Himalaya) have not been reported from the study area. Paucity of Pre-Himalayan deformation signatures could be due to obliteration of such features, if any, by intense Himalayan deformation along such major thrusts in the Himalaya. In another example, Bhargava et al. (2011) document pre-Tethyan deformation based on field observations along the Dharagad Thrust in the Tons valley, Lesser Himalaya in Himachal Pradesh, India. Top-to-S/SW shear has been proved conclusively to be the Himalayan or collision induced deformation signature based on sigmoidal-/lensoidal foliations, S-C fabrics, asymmetric porphyroclasts, sheared quartz veins, mineral fish, intrafolial folds etc. (e.g., Brunel, 1986; Herren, 1987; Grasemann et al., 1999; Jain et al., 2002; Mukherjee and Koyi, 2010). Hence, the analyses made with the chosen vein samples reflect the MBT-related related-order deformations. Veins not giving shear sense have been avoided in this study (Repository Fig. 3). Cross-fractures and boudin necks (as in Fig. 3c) indicate the syntectonic nature of the veins (such as Fig. 3 of Beach and Jack, 1982), and we utilized them in the present analyses. The studied veins are not the products of hydro-fracturing since they lack the typical network of vein as in Fig. 7b of Bons et al. (2012). Further, these veins are not the post-tectonic fill ups, since the typical tooth-like individual geometries of grains (Fig. 1a of Bons et al., 2012) are never encountered. Due to lack of crystal preferred orientation/growth direction of the grains inside the veins, the syntaxial/anataxial/epitaxial nature (Okamoto and Sekine, 2011; Bons et al., 2012) of the studied veins cannot be deciphered, but is neither relevant in this study.

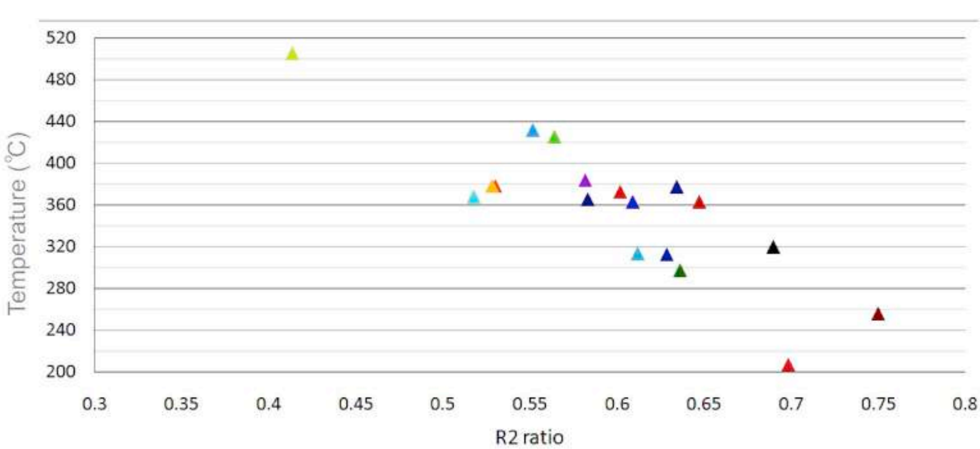

Fig. 9. Temperature calculated from the equation given by Rahl et al. (2005).

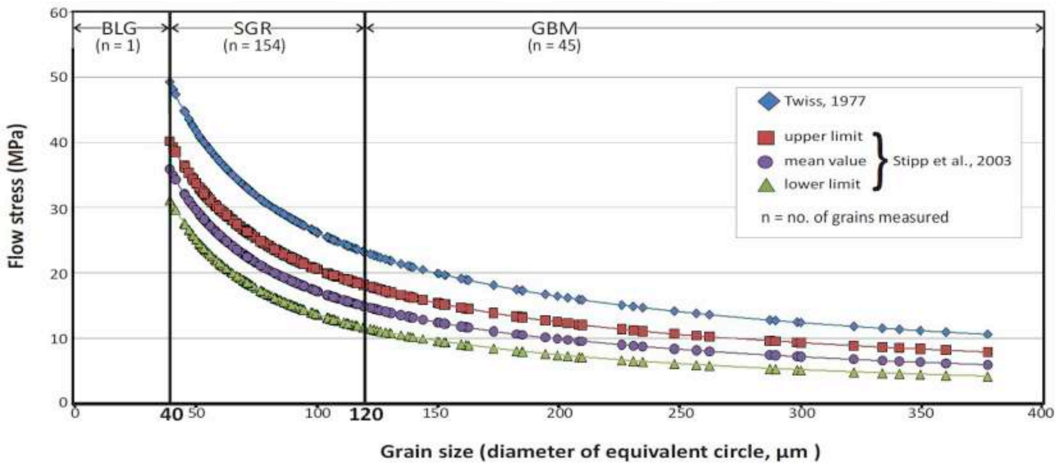

Fig. 10. Experimental results plotted in a grain size vs. flow stress diagram. Division of BLG, SGR, GBM zones has been done according to Stipp et al. (2010).

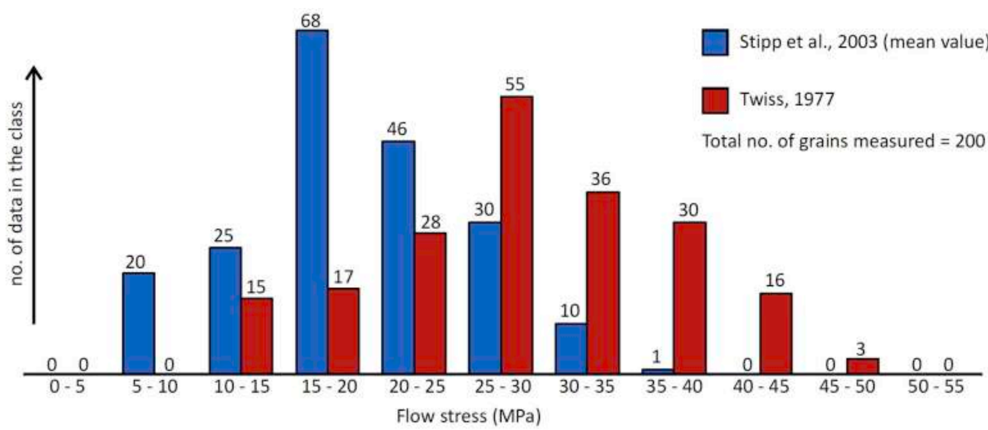

Fig. 11. Frequency distribution of experimental data in various classes of flow-stress.

Table 1
Results of piezometric experiments and strain-rates calculated from them.

Nature of Deformation	Temperature (K)	Pressure (MPa) (experimental results)	Strain rate (s-1)
BLG-SGR transition (grain size ~ 40 µm)	673	49.18[a] 35.88 ± 4.45[b]	1.23E-15 3.48E-16
SGR-GBM transition (grain size ~ 120 µm)	773	23.32[a] 15.02 ± 3.20[b]	1.40E-15 2.43E-16

[a] Measured as per Twiss (1977).
[b] Measured as per Stipp and Tullis (2003).

5.2. Clays and phyllonitization

Clay and phyllosilicate-rich shear zones have been reported from various geologic settings, such as clay-filled fractures, lithospheric detachments, accretionary prisms, subduction zones, continental shelves, fold-thrust belts and along several extensional and strike slip regimes (Warr and Cox, 2001 and references therein; Buatier et. al. 2012; Lacroix et al., 2012). In fault zones, clay precipitates from fluids flowing fractures (Warr and Cox, 2001; Lacroix et al., 2012, 2013). The petrophysical properties of fault planes are affected by syn-deformational growth of clay minerals, viz., clinochlore and illite (Lacroix et al., 2013; Bose and Bhattacharya, 2013). There are three possible geneses of clay minerals in fault zones (Warr and Cox, 2001): *(i)* anhydrous cataclasis and frictional melting, *(ii)* hydrous chloritisation of mafic minerals, and *(iii)* growth of swelling clay in the matrix.

Clays significantly decrease the shear strength of fault zones. For example-the shear strength of schists or slates are ~0.38 MPa, whereas it reduces drastically to 0–0.18 MPa for clay-filled shear planes at the Alpine Fault zone (Warr and Cox, 2001). It can happen dominantly by the two following ways (Warr and Cox, 2001; Buatier et al. 2012). *(i)* Due to micro-pores and considerable amount of void spaces in their crystal structures, clays can either absorb or release voluminous fluids, various cations, organic matters held in them during hydration-dehydration reactions and seismic events. This phenomenon greatly affects the fluid pressure of the fault zone. Increased fluid pressure in the fault zone decreases its strength. *(ii)* Compared to other rock forming minerals, clays deform more easily by dislocation glide along cleavages. Low frictional coefficient along such weak slip surfaces leads to aseismic creep.

The clay minerals present in the studied samples (clinochlore and illite) plausibly play similar roles in the deformation. But, providing further proof to that is beyond the scope of current study. However, presence of clays and intense shear indicate phyllonitisation (Knopf, 1931; review in White, 2010) of the Chandpur phyllites in the studied part of the MBT zone. Such low-grade phyllonites have been reported ubiquitously at the base of thrust sheets (e.g., Gray, 1995; Corfu and Heim, 2013; Bhattacharyya and Mitra, 2014) and experience a < 500 °C peak metamorphic temperature (Foster et al., 2009). These information match well with the current study, as the phyllonite is present at the base of MBT sheet and shows a peak metamorphic temperature of ~500 °C.

5.3. Thermometry

In this study both the host phyllite and the quartz veins present in them underwent the same MBT-related deformations indicated by the common top-to-S shear (Fig. 2). The quartz microstructure thermometry indicates the deformation temperature, whereas the LRSCM thermometry done on the carbonaceous material present in the phyllites connotes peak metamorphic temperature. According to Stipp et al. (2002) and Passchier and Trouw (2005), for quartz the transitions: cataclastic flow to BLG, BLG to SGR, and SGR to GBM takes place ~ 300, 400, and 500 °C, respectively. Hence, the mean of peak metamorphic temperatures obtained by LRSCM, i.e.,~374 °C and ~356 °C show a good correlation with the thermometric data obtained by the quartz deformation thermometry.

The Pelling-Munsiari thrust in the Sikkim Lesser Himalaya, which formed at a much higher structural level had only 360 °C recorded at its leading edge and 410 °C at its at its trailing edge (Bhattacharyya and Mitra, 2014). However, a direct comparison between this known information in eastern Himalaya with what we derive in western Himalaya is implausible since several other tectonic parameters such as slip rate of major thrusts and exhumation rates of the mountain chain vary significantly along the Himalayan trend (review in Mukherjee, 2013). Célérier et al. (2009b) measure a peak metamorphic temperature < 300 °C from the LRSCM study of the nearby MBT hanging wall rocks of Outer-LHS in the Garhwal Himalaya. Studying the quartz-feldspar microstructures, Long et al. (2011) calculate a 250–310 °C deformation temperature for the Lesser Himalayan rocks in Bhutan. The LRSCM method revealed that the Nepalese Lesser Himalaya experienced 540-330 °C metamorphic temperature (Beyssac et al., 2004). Using the LRSCM technique, Mathew et al. (2013) estimated deformation temperature of 240–300 °C for the MBT zone rocks of the Arunachal Himalaya, India. A conclusive comparison between the known temperature data from LHS from different locations of the Himalaya with the present data would not be possible.

5.4. Piezometry

The flow stress depends on the sizes of the recrystallised quartz grains (Stipp and Tullis, 2003). After nucleation, the size of the recrystallised quartz grains remains unchanged and does not depend on temperature (Xia and PlattJ, 2018). Geologically active thrust zones, such as the study area in current study, experiences temporally variable differential stress/flow stress (10–500 MPa) during its evolution through multiple seismic-aseismic cycles (e.g., Hawemann et al., 2018). The 39.89–376.82 μm range of grain sizes measured in this study also indicates a variable flow stress condition in the study area.

The final steady state product of any incremental dynamic deformation is preserved in thin sections. Thus, this measurement of flow stress gives an idea about the final products only, and not the whole dynamic deformation procedure. The steady state recrystallised grain sizes increase presumably by later deformations, otherwise the measurement will underestimate the original value (Stipp and Tullis, 2003). To overcome this problem, Twiss (1977) points out that the recrystallised grain sizes can be preserved by three mechanisms, one of which is the constant tectonic plate-induced stress accompanied by slow cooling rate. We consider such a condition to prevail in the study region since the MBT activated (e.g., Burbank et al., 2003). Hence, Twiss' idea would apply in the present study. Stipp et al. (2010)'s piezometer (Eqns. (4) and (5) in Section 3.4) gives a satisfactory range of deformation temperature for the SGR range. But for high temperature ranges like the GBM, it underestimates the flow stress magnitude, which can be considered as the minimum stress estimate for these zones. Although numerous grains below the measured range were found, it was difficult to measure their areas properly for their submicroscopic sizes. The numerous small BLG recrystallised grains present in the sample were not measured. From these points of views, the flow stress measured for the SGR recrystallisation deformation appears to be most reliable and is adopted in this study.

5.5. Strain rate estimation

The grain sizes related to the transition zones amongst the BLG, the SGR and the GBM domains were empirically given by Stipp et al. (2010). Related temperature values can be found from Passchier and Trouw (2005). Using the experimentally derived flow stress data, the strain rate values were calculated for the SGR recrystallisation zone.

In this study, the flow stress magnitudes calculated from the equations of Twiss (1977) and Stipp and Tullis (2003) (eqns. (4) and (5) in Section 3.4) yield strain rates $10^{-15}$to 10^{-16} s^{-1}. In general, the strain rates in natural shear zones range 10^{-13}-10^{-15} s^{-1} (Pfiffner and Ramsay, 1982; Ragan, 2009; review in Fagereng and Biggs, 2019). Strain rate in collisional orogens range 10^{-12} to 10^{-18} s^{-1} (Hobbs et al., 1976 and references therein). A different estimate from GPS studies provides a range of 10^{-13} to 10^{-11} s^{-1} (review in Lu and Jiang, 2019). Strain rates $\sim 10^{-15}$ s^{-1} or lower matches well with the results of viscous sheet models for various continents (references in table 1 of Fagereng and Biggs, 2019). In a tectonically active region, multiple earthquake cycles, as expected in the collisional orogens such as the Himalaya, produce an average strain rate of $\leq 10^{-15}$ s^{-1} (Fagereng and Biggs, 2019). A low strain rate an indicate seismicity (Campbell et al., 2015; Christophersen et al., 2017). The current study deduces such a value, however one should note that the deduced strain rate need not be the present day strain rate along the MBT. GPS-derived strain rate from the MBT, Garhwal or the Mussourie region in particular in our study area is sparse. Only Khandelwal et al. (2014) report the present day annual variation of strain to be ± 4 mm on horizontal component. Sharma and Lindholm (2012) modelled seismicity in MBT in the Dehradun region as Poisson earthquake distribution. Monalisa and Khwja (2005) commented that the MBT in the NW Indian (and also in Pakistan) is overall seismic. On the other hand, the seismic zonation map of India shows a high to very high chance of earthquake in the north part of Uttarakhand state that includes our study area (see Fig. 5 of Verma and Bansal, 2013). More specifically, Fig. 1 of Joshi and Kumar (2010) shows earthquakes of $M < 4$ plots at some parts of MBT in the Uttarakhand state. The GPS data indicates that the present day strain rate in the Indian subcontinent is $< 10^{-14}$ s^{-1} (Ader et al., 2012). Studying the zoning in garnets from Lesser Himalaya of central Nepal, Kohn et al. (2004) decipher that the strain rates along the local faults varies in the geological time range (10^3–10^6 years). From quartz dislocation creep, Francsis (2012) documents 10^{-12}-10^{-14} s^{-1} of strain rate near the Main Central Thrust (MCT) in the Sutlej valley, India. Hence, the strain rate values generated in this study matches with previous studies. It can also be inferred that, deformation (or, strain accumulation) along the MBT for some time period was less than the deformation (or, strain accumulation) along the MCT. Because of sparse data, it is implausible to comment whether strain rate varies systematically towards the foreland side of the Himalayan collisional orogen.

6. Conclusions

I. Clay minerals like chlinochlore and illite are the evidences of enhanced fluid activity in this fault zone. Those minerals are likely to influence the strength of fault zones and play a key role in controlling the fluid pressure.

II. Brittle deformed quartz as well as all the three dynamically recrystallised zones (i.e., the BLG, the SGR and the GBM recrystallised zones) co-exist the thin-section samples. Hence, the maximum estimates of the deformation temperature, from < 300 °C to > 500 °C, is predicted from the quartz deformation thermometry. During dynamic recrystallisation, presence of fluid indulges grain boundary microstructures to be present at temperatures lower than the expected. Previous works indicate that phyllites are common at the base of a thrust sheet and deforms at < 500 °C.

III. Laser Raman spectroscopy of carbonaceous materials estimates~356–374 (±50) °C of peak metamorphic temperature. When compared with the previously obtained results from the Lesser Himalaya, this study plausibly indicates shear heating at the base of the MBT thrust sheet.

IV. Recrystallised quartz grain size-based piezometry estimates the flow stress range ~6–49 MPa indicating a temporally variable range of tectonic stress conditions through geological time.

V. Based on available data and experimental results, this study estimates a strain rate of the order 10^{-15} or 10^{-16} s^{-1}, which is nearly matching with the strain rate values obtained from other Himalayan thrusts as well as natural shear zones.

Acknowledgements

Michael Stipp clarified few points. Hari Shankar Pandalai and George Mathew clarified issues related to the laser Raman spectroscopy. Spectra generation and baseline correction was assisted by Shilpa V. Netravali. Suggestions from Trupti V. Chandrasekhar regarding the XRD analysis were useful. We thank the Handling Editor Adam Bumby and the two anonymous reviewers for constructive and detail comments. SM acknowldges internal research funding from IIT Bombay. Efforts by previous handling editors (Ian Alsop and Arkoprobho Biswas) and reviewers (Kathakali Bhattacharyya and three anonymous persons) in different platforms greatly improved the article.

Declaration of competing interest

No conflict of interest.

Appendix 1

The fundamentals of Laser Raman Spectroscopy have been described elsewhere (Beyssac et al., 2002, 2003; Bradley, 2007; Chipara et al., 2011 etc). The Laser Raman Spectroscopy of the carbonaceous materials generates characteristic peaks D1, D2 and G, plotted in a 2D graph the Raman shift (cm^{-1}) along the X-axis and absolute counts of intensity along the Y-axis. The positions and intensity of these D1, D2 and G peaks represent the order in the structure of the carbonaceous material and hence provides clue to estimate the peak metamorphic temperature (e.g., Nibourel et al., 2018).

Appendix 2

Poirier's (1985) experiments on monophase and polyphaser aggregates give the following equation:

$$\dot{\varepsilon} = Ad^{-m}\sigma^{n} \exp\left(\frac{-Q}{RT}\right) \tag{8}$$

Here $\dot{\varepsilon}$: steady-state strain rate, A: pre-exponential factor, σ: differential flow stress, n: stress exponent, Q: apparent activation energy, R: gas constant, T: absolute temperature (K), d: grain size, m: grain size exponent.

Experimenting with olivine-pyroxene rich rocks, Tsenn and Carter (1987) present the following formula:

$$\dot{\varepsilon} = A \exp\left(\frac{-Q}{RT}\right)\exp(\beta\sigma) \tag{9}$$

Here $\dot{\varepsilon}$: steady-state strain rate, Q: apparent activation energy, R: gas constant, T: absolute temperature (K), β: empirical constant, σ: differential flow stress.

Neither eqn (1) nor eqn (2) incorporate various natural parameters (e.g. water fugacity), resulting in oversimplification of the models (Kirby and Kronenberg, 1987; Kohlstedt et al., 1995; Blenkinsop, 2007).

Appendix 3. Table 1 (Submitted as a Repository File since it is of a slightly different format and is not coming in this place)

.

Appendix A. Supplementary data

Supplementary data to this article can be found online at https://doi.org/10.1016/j.marpetgeo.2019.104094.

References

Acharyya, S.K., Ray, K.K., 1982. Hydrocarbon possibilities of concealed Mesozoic-Paleogene sediments below Himalayan-nappes- reappraisal. AAPG Bull. 66, 57–70.
Ader, T., Avouac, J.P., Liu-Zeng, J., Lyon-Caen, H., Bollinger, L., Galetzka, J., Thomas, M., Chanard, K., Sapkota, S.N., Rajaure, S., Shrestha, P., Ding, L., Flouzat, M., 2012. Convergence rate across the Nepal Himalaya and interseismic coupling on the main Himalayan thrust: implications for seismic hazard. J. Geophys. Res.: Solid Earth 117B04403.
Arch, J., Maltman, A.J., Knipe, R.J., 1988. Shear-zone geometries in experimentally deformed clays: the influence of water content, strain rate and primary fabric. J. Struct. Geol. 10, 91–99.
Austin, N.J., 2011. The microstructural and rheological evolution of shear zones. In: In: Prior, D.J., Rutter, E.H., Tatham, D.J. (Eds.), Deformation Mechanisms, Rheology and Tectonics: Microstructures, Mechanics and Anisotropy, vol. 360. Geol. Soc. London Sp. Pubs, pp. 193–209.
Beach, A., Jack, S., 1982. Syntectonic vein development in a thrust sheet from the external French Alps. Tectonophysics 81, 67–84.
Beyssac, O., Goffé, B., Chopin C andRouzaud, J.N., 2002. Raman spectra of carbonaceous material in metasediments: a new geothermometer. J. Metamorph. Geol. 20, 859–871.
Beyssac, O., Goffé, B., Petitet, J.P., Froigneux, E., Moreau, M., Rouzaud, J.N., 2003. The characterization of disordered and heterogenous carbonaceous materials by Raman spectroscopy. Spectrochim. Acta, Part A 59, 2267–2276 On.
Beyssac, O., Bollinger, L., Avouac, J.P., Goffé, B., 2004. Thermal metamorphism in the lesser Himalaya of Nepal determined from Raman spectroscopy of carbonaceous material. Earth Planet. Sci. Lett. 225, 233–241.
Bhargava, O.N., Frank, W., Bertle, R., 2011. Late cambrian deformation in the lesser Himalaya. J. Asian Earth Sci. 40, 201–212.
Bhat, G.M., Craig, J., Hafiz, M., Hakhoo, N., Thurow, J.W., Thusu, B., Cozzi, A., 2012. Geology and hydrocarbon potential of neoproterozoic–cambrian basins in Asia: an introduction. In: In: Bhat, G.M., Craig, J., Thurow, J.W., Thusu, B., Cozzi, A. (Eds.), 2012. Geology and Hydrocarbon Potential of Neoproterozoic–Cambrian Basins in Asia, vol. 366. Geological Society, London, Special Publications, pp. 1–17.
Bhattacharya AR. (Internet reference) Himalayan deformation: implications for

hydrocarbon exploration. URL: file:///C:/Users/Guest/Downloads/lecture-technical-details%20(2).pdf (Accessed on 25-May-2019).
Bhattacharyya, K., Mitra, G., 2011. Strain softening along the MCT zone from the Sikkim Himalaya: relative roles of quartz and micas. J. Struct. Geol. 33, 1105–1121.
Bhattacharyya, K., Mitra, G., 2014. Spatial variations in deformation mechanisms along the Main Central thrust zone: implications for the evolution of the MCT in the Darjeeling–Sikkim Himalaya. J. Asian Earth Sci. 96, 132–147.
Blenkinsop, T.G., 2007. Deformation Microstructures and Mechanisms in Minerals and Rocks. Springer Science & Business Media, Dordrecht (Netherlands), pp. 90.
Blenkinsop, T.G., 2008. Relationships between faults, extension fractures and veins, and stress. J. Struct. Geol. 30, 622–632.
Boncio, P., 2008. Deep-crust strike-slip earthquake faulting in southern Italy aided by high fluid pressure: insights from rheological analysis. In: In: Wibberley, C.A.J., Kurz, W., Imber, J., Holdsworth, R.E., Collettini, C. (Eds.), The Internal Structure of Fault Zones: Implications for Mechanical and Fluid-Flow Properties, vol. 299. Geol. Soc. London Sp. Pubs, pp. 195–210.
Bons, P.D., Elburg, M.A., Gomez-Rivas, E., 2012. A review of the formation of tectonic veins and their microstructures. J. Struct. Geol. 43, 33–62.
Bose, N., Bhattacharya, G., 2013. A rare microstructure: trapezoid-shaped aggregate of fine-grained minerals. Int. J. Earth Sci. 103, 1057.
Bose, N., Mukherjee, S., 2019a. Field documentation and genesis of the back-structures from the garhwal lesser Himalaya, Uttarakhand, India, tectonic implications. In: In: Sharma, Villa, I.M., Kumar, S. (Eds.), Crustal Architecture and Evolution of the Himalaya-Karakoram-Tibet Orogen, vol. 481. Geological Society of London Special Publications, pp. 111–125.
Bose, N., Mukherjee, S., 2019b. Field documentation and genesis of back-structures in ductile and brittle regimes from the foreland part of a collisional orogen: examples from the Darjeeling–Sikkim Lesser Himalaya, India. Int. J. Earth Sci. 108, 1333–1350.
Bose, N., Dutta, D., Mukherjee, S., 2018. Role of grain-size in phyllonitisation: insights from mineralogy, microstructures, strain analyses and numerical modeling. J. Struct. Geol. 112, 39–52.
Boulton, C., Davies, T., McSaveney, M., 2009. The frictional strength of granular fault gouge: application of theory to the mechanics of low-angle normal faults. In: In: Ring, U., Wernicke, B. (Eds.), Extending a Continent: Architecture, Rheology and Heat Budget, vol. 321. Geol. Soc. London Sp. Pubs., pp. 9–31.
Boutonnet, E., Leloup, P.H., Sassier, C., Gardien, V., Ricard, Y., 2013. Ductile strain rate measurements document long-term strain localization in the continental crust. Geology 41, 819–822.
Bradley, M., 2007. Curve Fitting in Raman and IR Spectroscopy: Basic Theory of Line Shapes and Applications. Thermo Fisher Scientific, Madison, USA, Application Note, pp. 50733.
Brunel, M., 1986. Ductile thrusting in the Himalayas: shear sense criteria and stretching lineations. Tectonics 5, 247–265.
Buatier, M.D., Lacroix, B., Labaume, P., Moutarlier, V., Charpentier, D., 2012. Sizun J P andTravé A 2012 Microtextural investigation (SEM and TEM study) of phyllosilicates in a major thrust fault zone (Monte Perdido, southern Pyrenees): impact on fault reactivation. Swiss J. Geosci. 105, 313–324.
Burbank, D.W., Blythe, A.E., Putkonen, J., Pratt-Sitaula, Gabet, E., Oskin, M., Barros, A., Ojha, T.P., 2003. Decoupling of erosion and precipitation in the Himalayas. Nature 426, 652–655.
Campbell, G.E., Walker, R.T., Abdrakhmatov, K., Jackson, J., Elliott, J.R., Mackenzie, D., Middleton, T., Schwenninger, J.L., 2015. Great earthquakes in low strain rate continental interiors: an example fromSE Kazakhstan. J. Geophys. Res.: Solid Earth 120. https://doi.org/10.1002/2015JB011925.
Cavalcante, C., Lagoeiro, L., Fossen, H., Egydio-Silva, M., Morales, L.F., Ferreira, F., Conte, T., 2018. Temperature constraints on microfabric patterns in quartzofeldspathic mylonites, Ribeira belt (SE Brazil). J. Struct. Geol. 115, 243–262.
Célérier, J., Harrison, T.M., Beyssac, O., Herman, F., Dunlap, W.J., Webb, A.A.G., 2009a. The Kumaun and garwhal lesser Himalaya, India: Part 1. Structure and stratigraphy. Geol. Soc. Am. Bull. 121, 1262–1280.
Célérier, J., Harrison, T.A., Webb, A.A.G., Yin, A., 2009b. The Kumaun and garwhal lesser Himalaya, India: Part 2. Thermal and deformation histories. Geol. Soc. Am. Bull. 121, 1281–1297.
Chipara, D.M., Chipara, A.C., Chipara, M., 2011. Raman spectroscopy of carbonaceous materials: a concise review. Spectrosc. Eur. 26, 42.
Christie, J.M., Ord, A., 1980. Flow stress from microstructures of mylonites: example and current assessment. J. Geophys. Res.: Solid Earth 85, 6253–6262.
Christophersen, A., Rhoades, D.A., Colella, H.V., 2017. Precursory seismicity in regions of low strain rate: insights from a physics-based earthquake simulator. Geophys. J. Int. 209, 1513–1525.
Coli, M., Sani, F., 1990. Vein distribution in a thrust zone: a case history from the Northern Apennines, Italy. In: In: Knipe, R.J., Rutter, E.H. (Eds.), Deformation Mechanisms, Rheology and Tectonics, vol. 54. Geol. Soc. London Sp. Pubs, pp. 475–482.
Cooper, M., 2007. Structural style and hydrocarbon prospectivity in fold and thrust belts: a global review. In: Ries, A.C., Butler, R.W.H., Graham, R.H. (Eds.), Deformation of the Continental Crust: the Legacy of Mike Coward. Geological Society, London, Special Publications 272, pp. 447–472.
Corfu, F., Heim, M., 2013. Geology and U–Pb geochronology of the Espedalen Complex, southern Norway, and its position in the Caledonian nappe systems. In: In: Corfu, F., Gasser, D., Chew, D.M. (Eds.), New Perspectives on the Caledonides of Scandinavia and Related Areas, vol. 390. Geol. Soc. London Sp. Pubs, pp. 223–239.
Cox, S.F., 1998. Vein development in reverse fault zones. In: Snoke, A.W., Tullis, J., Todd, V.R. (Eds.), Fault-related Rocks: A Photographic Atlas. Princeton University Press, New Jersey, 0-691-01220-2, pp. 3–18.
Craig, J., Hakhoo, N., Hafiz, M., Khan, M.R., Misra, R., Pandita, S.K., Raina, B.K., Thurow, J., Thusu, B., Ahmed, W., Khullar, S., 2018. Petroleum systems and hydrocarbon potential of the North-West Himalaya of India and Pakistan. Earth-Sci. Rev. 187, 109–185.
Degen, T., Sadki, M., Bron, E., König, U., Nénert, G., 2014. The HighScore suite. Powder Diffr. 29, 13–18.
Draganits, E., Grasemann, B., Hager, C., 2005. Conjugate, cataclastic deformation bands in the Lower Devonian Muth Formation (Tethyan Zone, NW India): evidence for pre-Himalayan deformation structures. Geol. Mag. 142, 765–781.
Drury, M.R., 2005. Dynamic recrystallization and strain softening of olivine aggregates in the laboratory and the lithosphere. In: In: Gapais, D., Brun, J.P., Cobbold, P.R. (Eds.), Deformation Mechanisms, Rheology and Tectonics: from Minerals to the Lithosphere, vol. 243. Geol. Soc. London Sp. Pubs., pp. 143–158.
Dutta, D., Biswas, T., Mukherjee, S., 2019. Arc-parallel compression in the NW Himalaya: evidence from structural and palaeostress studies of brittle deformation from the clasts of the Upper Siwalik, Uttarakhand, India. J. Earth Syst. Sci. 128. https://doi.org/10.1007/s12040-019-1138-1.
Evans, J.P., 1990. Textures, deformation mechanisms, and the role of fluids in the cataclastic deformation of granitic rocks. In: In: Knipe, R.J., Rutter, E.H. (Eds.), Deformation Mechanisms, Rheology and Tectonics, vol. 54. Geol. Soc. London Spec. Publ, pp. 29–39.
Fagereng, Å., Biggs, J., 2019. New perspectives on 'geological strain rates' calculated from both naturally deformed and actively deforming rocks. J. Struct. Geol. 125, 100–110.
Farrell, K., 2017. Characterising the Deep Structure and Seismic Signature of an Exhumed Ductile Shear Zone. Doctoral dissertation, University of Leeds, pp. 1–226.
Fossen, H., 2016. Structural Geology, second ed. Cambridge University Press, pp. 463.
Foster, D.A., Goscombe, B.D., Gray, D.R., 2009. Rapid exhumation of deep crust in an obliquely convergent orogen: the Kaoko Belt of the Damara Orogen. Tectonics 28, 1–24 TC4002.
Francsis, M.K., 2012. In: Piezometry and Strain Rate Estimates along Mid-crustal Shear Zones. Virginia Polytechnic Institute, pp. 110 Master's thesis.
Garzanti, E., Jadoul, F., Nicora, A., Berra, F., 1995. Triassic of Spiti (Tethys Himalaya, N India). Riv. Ital. Paleontol. Stratigr. 101, 267–300.
Ghose, A., 2006. Metallogenic Characteristics in Relation to Tectonic Framework of the Himalaya, vol. 132. Memoirs Geological Survey of India, Kolkata, pp. 1–232.
Goscinak, C.J., 2014. Quartz Fabric Analysis of the Kawishiwi Shear Zone, NE Minnesota. Master's thesis. University of Minnesota, pp. 1–46.
Grasemann, B., Fritz, H., Vannay, J.C., 1999. Quantitative kinematic flow analysis from the Main Central Thrust Zone (NW-Himalaya, India): implications for a decelerating strain path and the extrusion of orogenic wedges. J. Struct. Geol. 21, 837–853.
Gray, D.R., 1995. Thrust kinematics and transposition fabrics from a basal detachment zone, eastern Australia. J. Struct. Geol. 17, 1637–1654.
Griggs, D., 1967. Hydrolytic weakening of quartz and other silicates. Geophys. J. Int. 14, 19–31.
Gueydan, F., Mehl, C., Parra, T., 2005. Stress-strain rate history of a midcrustal shear zone and the onset of brittle deformation inferred from quartz recrystallized grain size. Geol. Soc. Lond. Spec. Publ. 243, 127–142.
Haertel, M., Herwegh, M., Pettke, T., 2013. Titanium-in-quartz thermometry on synkinematic quartz veins in a retrograde crustal-scale normal fault zone. Tectonophysics 608, 468–481.
Hakhoo, N., Thusu, B., Mani, D., Bhat, G.M., 2016. Hydrocarbon source potential of the proterozoic sirban limestone formation, NW Himalaya, Jammu. J. Geol. Soc. India 88, 685–692.
Handy, M.R., 1989. Deformation regimes and the rheological evolution of fault zones in the lithosphere: the effects of pressure, temperature, grain size and time. Tectonophysics 163, 119–152.
Handy, M.R., 1994. Flow laws for rocks containing two non-linear viscous phases: a phenomenological approach. J. Struct. Geol. 16, 287–302.
Hawemann, F., Mancktelow, N.S., Pennacchioni, G., Wex, S., Camacho, A., 2018. Weak and slow, strong and fast: how shear zones evolve in a dry continental crust (Musgrave Ranges, Central Australia). J. Geophys. Res.: Solid Earth. https://doi.org/10.1029/2018JB016559.
Henderson, I.H.C., McCaig, A.M., 1996. Fluid pressure and salinity variations in shear zone-related veins, central Pyrenees, France: implications for the fault-valve model. Tectonophysics 262, 321–348.
Herren, E., 1987. Zanskar shear zone: northeast-southwest extension within the higher Himalayas (Ladakh, India). Geology 15, 409–413.
Hirth, G., Tullis, J., 1992. Dislocation creep regimes in quartz aggregates. J. Struct. Geol. 14, 145–159.
Hirth, G., Teyssier, C., Dunlap, W.J., 2001. An evolution of quartzite flow laws based on comparisons between experimentally & naturally deformed rocks. Int. J. Earth Sci. 90, 77–87.
Hobbs, B.E., Means, W.D., Williams, P.F., 1976. An Outline of Structural Geology. John Wiley& Sons, New York, 0-471-40157-9pp. 472.
Hu, S., Evans, K., Craw, D., Rempel, K., Bourdet, J., Dick, J., Grice, K., 2015. Raman characterization of carbonaceous material in the Macraes orogenic gold deposit and metasedimentary host rocks, New Zealand. Ore Geol. Rev. 70, 80–95.
Hunter, N.J., Weinberg, R.F., Wilson, C.J., Luzin, V., Misra, S., 2018. Microscopic anatomy of a "hot-on-cold" shear zone: insights from quartzites of the main central thrust in the Alaknanda region (Garhwal Himalaya). Geol. Soc. Am. Bull. 130, 1519–1539.
Islam, R., Ghosh, S.K., Vyshnavi, S., Sundriyal, Y.P., 2011. Petrography, geochemistry and regional significance of crystalline klippen in the Garhwal Lesser Himalaya, India. J. Earth Syst. Sci. 120, 489–501.
Jain, A.K., Singh, S., Manickavasagam, R.M., 2002. Himalayan collision tectonics. Gondwana Research Group, pp. 1–114 Memoir 7, 4-938925-13-3-C3344.
Jayangondaperumal, R., Dubey, A.K., 2001. Superposed folding of a blind thrust and

formation of klippen: results of anisotropic magnetic susceptibility studies from the Lesser Himalaya. J. Asian Earth Sci. 19, 713–725.
Jayangondaperumal, R., Thakur, V.C., Joevivek, V., Rao, P.S., Gupta, A.K., 2018. Active Tectonics of Kumaun and Garhwal Himalaya. Springer Natural Hazards, 978-981-10-8243-6pp. 30.
Ji, S., Xia, B., 2002. Rheology of polyphase Earth materials. Polytechnique International Press, 2-553-01033-8pp. 10 13.
Jiang, G., Christile-Blick, N., Kaufman, A.J., Banerjee, D.M., Rai, V., 2002. Sequence stratigraphy of the neoproterozoic infra Krol formation and Krol group, lesser Himalaya, India. J. Sediment. Res. 72, 524–542.
Joshi, G.C., Kumar, R., 2010. Preliminary seismic vulnerability assessment of Mussoorie town, Uttarakhand (India). J. Build. Apprais. 5, 357–368.
Joshi, B.C., Singh, B., Dikshit, V.N., 2011. Study of Landslide Occurrence along Main Boundary Thrust and its Impact in Dehradun Region - A Report. INDOROCK 2011. Third Indian Rock Conference by Indian Society for Rock Mechanics and Tunnelling Technology 397-373.
Kali, E., Leloup, P.H., Arnaud, N., Mahéo, G., Liu, D., Boutonnet, E., van der Woerd, J., Liu, X., Liu-Zeng, J., Li, H., 2010. Exhumation history of the deepest central Himalayan rocks, Ama Drime range: key pressure-temperature-deformation-time constraints on orogenic models. Tectonics 29, TC2014. https://doi.org/10.1029/2009TC002551.
Khandelwal, D.D., Gahalaut, V., Kumar, N., Kundu, B., Yadav, R.K., 2014. Seasonal variation in the deformation rate in NW Himalayan region. Nat. Hazards 74, 1853–1861.
Kirby, S.H., Kronenberg, A.K., 1987. Rheology of the lithosphere: selected topics. Rev. Geophys. 25, 1219–1244.
Knopf, E.F.B., 1931. Retrogressive metamorphism and phyllonitization. Am. J. Sci. 121, 1–27.
Kohlstedt, D.L., Evans, B., Mackwell, S.J., 1995. Strength of the lithosphere: constraints imposed by laboratory experiments. J. Geophys. Res.: Solid Earth 100, 17587–17602.
Kohn, M.J., Wieland, M.S., Parkinson, C.D., Upreti, B.N., 2004. Miocene faulting at plate tectonic velocity in the Himalaya of central Nepal. Earth Planet. Sci. Lett. 228, 299–310.
Kouketsu, Y., Mizukami, T., Mori, H., Endo, S., Aoya, M., Hara, H., Nakamura, D., Wallis, S., 2014. A new approach to develop the R aman carbonaceous material geothermometer for low-grade metamorphism using peak width. Isl. Arc 23, 33–50.
Krabbendam, M., Urai, J.L., van Vliet, L.J., 2003. Grain size stabilisation by dispersed graphite in a high-grade quartz mylonite: an example from Naxos (Greece). J. Struct. Geol. 25, 855–866.
Kruhl, J.H., Erdmann, S., Büttner, S.H., 2007. Brittle-ductile microfabrics in naturally deformed cordierite: evidence for significant short-term strain-rate variations. J. Struct. Geol. 29, 355–374.
Lacroix, B., Charpentier, D., Buatier, M., Vennemann, T., Labaume, P., Adatte, T., Travé, A., Dubois, M., 2012. Formation of chlorite during thrust fault reactivation. Record of fluid origin and P–T conditions in the Monte Perdido thrust fault (southern Pyrenees). Contrib. Mineral. Petrol. 163, 1083–1102.
Lacroix, B., Leclère, H., Buatier, M., Fabbri, O., 2013. Weakening processes in thrust faults: insights from the Monte Perdido thrust fault (southern Pyrenees, Spain). Geofluids 13, 56–65.
Law, R.D., 1990. Crystallographic fabrics: a selective review of their applications to research in structural geology. In: In: Knipe, R.J., Rutter, E.H. (Eds.), Deformation Mechanisms, Rheology and Tectonics, vol. 54. Geol. Soc. London Sp. Pub, pp. 335–352.
Law, R.D., 2014. Deformation thermometry based on quartz c-axis fabrics and recrystallization microstructures: a review. J. Struct. Geol. 66, 129–161.
Law, R.D., Stahr Iii, D.W., Francsis, M.K., Ashley, K.T., Grasemann, B., Ahmad, T., 2013. Deformation temperatures and flow vorticities near the base of the greater Himalayan series, Sutlej valley and Shimla Klippe, NW India. J. Struct. Geol. 54, 21–53.
Long, S., McQuarrie, N., Tobgay, T., Hawthorne, J., 2011. Quantifying internal strain and deformation temperature in the eastern Himalaya, Bhutan: implications for the evolution of strain in thrust sheets. J. Struct. Geol. 33, 579–608.
Lu, L.X., Jiang, D., 2019. Quartz flow law revisited: the significance of pressure dependence of the activation enthalpy. JGR Solid Earth 124, 241–256.
Ludwigson, D.C., 1971. Modified stress-strain relation for FCC metals and alloys. Metall. Trans. 2, 2825–2828.
Mamtani, M.A., Greiling, R.O., 2010. Serrated quartz grain boundaries, temperature and strain rate: testing fractal techniques in a syntectonic granite. In: In: Spalla, M.I., Marotta, A.M., Gosso, G. (Eds.), Advances in Interpretation of Geological Processes: Refinement of Multi-Scale Data and Integration in Numerical Modelling, vol. 332. Geol. Soc. London Sp. Pubs, pp. 35–48.
Mathew, G., De Sarkar, S., Pande, K., Dutta, S., Ali, S., Rai, A., Netrawali, S., 2013. Thermal metamorphism of the Arunachal Himalaya, India: Raman thermometry and thermochronological constraints on the tectono-thermal evolution. Int. J. Earth Sci. 102, 1911–1936.
Mazza, S.E., Mako, C., Law, R.D., Caddick, M.J., Krabbendam, M., Cottle, J., 2018. Thermobarometry of the moine and SgurrBeag thrust sheets, northern Scotland. J. Struct. Geol. 113, 10–32.
Mazzotti, S., Gueydan, F., 2018. Control of tectonic inheritance on continental intraplate strain rate and seismicity. Tectonophysics 746, 602–610.
Meigs, A.J., Burbank, D.W., Beck, R.A., 1995. Middle-late miocene (> 10 Ma) Formation of the main boundary thrust in the western Himalaya. Geology 23, 423–426.
Menant, A., Angiboust, S., Monié, P., Oncken, O., Guigner, J.M., 2018. Brittle deformation during Alpine basal accretion and the origin of seismicity nests above the subduction interface. Earth Planet. Sci. Lett. 487, 84–93.
Mishra, P., Mukhopadhyay, D.K., 2012. Structural evolution of the frontal fold–thrust belt, NW Himalayas from sequential restoration of balanced cross-sections and its hydrocarbon potential. Geol. Soc., Lond., Spec. Publ. 366, 201–228.
Monalisa Khwja, A.A., 2005. Seismic activity along the main boundary thrust (MBT), Pakistan. Geol. Bull. - Univ. Peshawar 38, 23–30.
Moore, D.M., Reynolds, R.C., 1989. X-ray Diffraction and the Identification and Analysis of Clay Minerals, vol. 378. Oxford University Press, New York, pp. 155.
Mukherjee, S., 2013. Channel flow extrusion model to constrain dynamic viscosity and Prandtl number of the Higher Himalayan Shear Zone. Int. J. Earth Sci. 102, 1811–1835.
Mukherjee, S., 2017a. Shear heating by translational brittle reverse faulting along a single, sharp and straight fault plane. J. Earth Syst. Sci. 126, 1–5.
Mukherjee, S., 2017b. Review on symmetric structures in ductile shear zones. Int. J. Earth Sci. 106, 1453–1468.
Mukherjee, B.K., Chakrabarti, M.K., 1996. Krol and infra Krol succession of Krol belt, lesser Himalayas – geology and hydrocarbon prospect. Drill. Explor. World J. 6, 159–176.
Mukherjee, S., Koyi, H.A., 2010. Higher Himalayan shear zone, Sutlej section- structural geology & extrusion mechanism by various combinations of simple shear, pure shear & channel flow in shifting modes. Int. J. Earth Sci. 99, 1267–1303.
Mukherjee, S., Carosi, R., van der Beek, P.A., Mukherjee, B.K., Robinson, D.M., 2015. Tectonics of the Himalaya: an introduction. In: In: Mukherjee, S., Carosi, R., van der Beek, P., Mukherjee, B.K., Robinson, D. (Eds.), Tectonics of the Himalaya, vol. 412. Geol. Soc. London Spec. Pub, pp. 1–3.
Mukherjee, S., Goswami, S., Mukherjee, A., 2019. Structures and their tectonic implications form the southern part of the Cuddapah basin, Andhra Pradesh, India. Iran. J. Sci. Technol. Trans. A-Science 43, 489–505.
Mulchrone, K.F., Mukherjee, S., 2016. Kinematics and shear heat pattern of ductile simple shear zones with 'slip boundary condition'. Int. J. Earth Sci. 105, 1015–1020.
Nabelek, P.I., Liu, M., Sirbescu, M.L., 2001. Thermo-rheological, shear heating model for leucogranite generation, metamorphism, and deformation during the Proterozoic Trans-Hudson orogeny, Black Hills, South Dakota. Tectonophysics 342, 371–388.
Nagy, A., Toth, T.M., 2012. Petrology and tectonic evolution of the Kiskunhalas-NE fractured hydrocarbon reservoir, South Hungary. Cent. Eur. Geol. 55/1, 1–22.
Newman, J., Mitra, G., 1994. Fluid-influenced deformation and recrystallization of dolomite at low temperatures along a natural fault zone, Mountain City window, Tennessee. Geol. Soc. Am. Bull. 106, 1267–1280.
Nibourel, L., Berger, A., Egli, D., Luensdorf, N.K., Herwegh, M., 2018. Large vertical displacements of a crystalline massif recorded by Raman thermometry. Geology 46, 879–882.
Ojha, P.S., 2012. Precambrian sedimentary basins of India: an appraisal of their petroleum potential. In: In: Bhat, G.M., Craig, J., Thurow, J.W., Thusu, B., Cozzi, A. (Eds.), 2012. Geology and Hydrocarbon Potential of Neoproterozoic–Cambrian Basins in Asia, vol. 366. Geol Soc, London, Spec Publications, pp. 19–58.
Okamoto, A., Sekine, K., 2011. Textures of syntaxial quartz veins synthesized by hydrothermal experiments. J. Struct. Geol. 33, 1764–1775.
Ord, A., Christie, J.M., 1984. Flow stresses from microstructures in mylonitic quartzites of the Moine Thrust zone, Assynt area, Scotland. J. Struct. Geol. 6, 639–654.
Panikkar, S.V., Subramanyan, V., 1996. A geomorphic evaluation of the landslides around Dehradun and Mussoorie, Uttar Pradesh, India. Geomorphology 15, 169–181.
Passchier, C.W., Trouw, R.A., 2005. Microtectonics, second ed. Springer, Berlin, pp. 366p.
Pathak, V., Pant, C.C., Darmwal, G.S., 2015. Geomorphological features of active tectonics and ongoing seismicity of northeastern Kumaun Himalaya, Uttarakhand, India. J. Earth Syst. Sci. 124, 1143–1157.
Pfiffner, O.A., Ramsay, J.G., 1982. Constraints on geological strain rates: arguments from finite strain states of naturally deformed rocks. J. Geophys. Res.: Solid Earth 87, 311–321.
Poirier, J.P., 1985. Creep of Crystals: High-Temperature Deformation Processes in Metals, Ceramics and Minerals. Cambridge University Press, New York, 9780521278515pp. 260.
Ponraj, M., Miura, S., Reddy, C.D., Prajapati, S.K., Amirtharaj, S., Mahajan, S.H., 2010. Estimation of strain distribution using GPS measurements in the Kumaun region of Lesser Himalaya. J. Asian Earth Sci. 39, 658–667.
Poppe, L.J., Paskevich, V.F., Hathaway, J.C., Blackwood, D.S., 2001. A laboratory manual for X-ray powder diffraction. US Geol. Surv. Open-File Rep. 1, 1–88.
Prescott, W.H., Savage, J.C., Kinoshita, W.T., 1979. Strain accumulation rates in the western United States between 1970 and 1978. J. Geophys. Res. Solid Earth 84, 5423–5435.
Quirico, E., Montagnac, G., Rouzaud, J.N., Bonal, L., Bourot-Denise, M., Duber, S., Reynard, B., 2009. Precursor and metamorphic condition effects on Raman spectra of poorly ordered carbonaceous matter in chondrites and coals. Earth Planet. Sci. Lett. 287, 185–193.
Ragan, D.M., 2009. Structural Geology: an Introduction to Geometrical Techniques, fourth ed. Cambridge University Press, pp. 402 -13 978-0-521-89758-7.
Rahl, J.M., Anderson, K.M., Brandon, M.T., Fassoulas, C., 2005. Raman spectroscopic carbonaceous material thermometry of low-grade metamorphic rocks: calibration and application to tectonic exhumation in Crete, Greece. Earth Planet. Sci. Lett. 240, 339–354.
Raina, B.N., 1978. A review of the stratigraphy and structure of Lesser Himalaya of Uttar Pradesh and Himachal Pradesh. In: Saklani, P.S. (Ed.), Tectonic Geology of the Himalaya. Today and Tomorrow's Printers & Publishers, New Delhi, pp. 63–78.
Ramola, R.C., Singh, S., Virk, H.S., 1988. Radon studies over main boundary thrust near Dehradun (India). Int. J. Radiat. Appl. Instrum. D Nucl. Tracks Radiat. Meas. 15, 617–619.
Ranalli, G., 1984. Grain size distribution and flow stress in tectonites. J. Struct. Geol. 6, 443–447.
Rao, R., 1986. North-west Himalayan foothills: its stratigraphical record and tectonic phases. Oil Nat. Gas Comm. Bull. 23, 109–128.
Rogowitz, A., Grasemann, B., Huet, B., Habler, G., 2014. Strain rate dependent calcite

microfabric evolution–An experiment carried out by nature. J. Struct. Geol. 69, 1–17.
Rutter, E.H., 1974. The influence of temperature, strain rate and interstitial water in the experimental deformation of calcite rocks. Tectonophysics 22, 311–334.
Sassier, C., Leloup, P.H., Rubatto, D., Galland, O., Yue, Y., Lin, D., 2009. Direct measurement of strain rates in ductile shear zones: a new method based on syntectonic dikes. J. Geophys. Res.: Solid Earth 114, 1–22. https://doi.org/10.1029/2008JB005597. B01406.
Schmid, S.M., 1982. Microfabric studies as indicators of deformation mechanisms and flow laws operative in mountain building. In: Hsu, K.J. (Ed.), Mountain Building Processes. Academic Press London, pp. 95–110.
Sharma, M.L., Lindholm, C., 2012. Earthquake hazard assessment for Dehradun, Uttarakhand, India, including a characteristic earthquake recurrence model for the Himalaya frontal fault (HFF). Pure Appl. Geophys. 169, 1601–1617.
Shen, Z.K., Jackson, D.D., Kagan, Y.Y., 2007. Implications of geodetic strain rate for future earthquakes, with a five-year forecast of M5 earthquakes in southern California. Seismol. Res. Lett. 78, 116–120.
Singh, S., Barley, M.E., Brown, S.J., Jain, A.K., Manickavasagam, R.M., 2002. SHRIMP U–Pb in zircon geochronology of the Chorgranitoid: evidence for Neoproterozoic magmatism in the Lesser Himalayan granite belt of NW India. Precambrian Res. 118, 285–292.
Singleton, J.S., Wong, M.S., Johnston, S.M., 2018. The Role of Calcite-Rich Metasedimentary Mylonites in Localizing Detachment Fault Strain and Influencing the Structural Evolution of the Buckskin-Rawhide Metamorphic Core Complex, West-Central Arizona; Lithosphere. https://doi.org/10.1130/L699.1.
Snoke, A.W., 1998. An overview of fault rocks. In: Snoke, A.W., Tullis, J., Todd, V.R. (Eds.), Fault-related Rocks: A Photographic Atlas. Princeton University Press, New Jersey, 0-691-01220-2, pp. 3–18.
Srivastava, P., Mitra, G., 1996. Deformation mechanisms and inverted thermal profile in the north Almora thrust mylonite zone, kumaon lesser Himalaya, India. J. Struct. Geol. 18, 27–39.
Stipp, M., Tullis, J., 2003. The recrystallized grain size piezometer for quartz. Geophys. Res. Lett. 30, 2088. https://doi.org/10.1029/2003GL018444.
Stipp, M., Stunitz, H., Heilbronner, R., Schmid, S.M., 2002. The eastern tonalite fault zone: a ‘natural laboratory’ for crystal plastic deformation of quartz over a temperature range from 250 to 700 °C. J. Struct. Geol. 24, 1861–1884.
Stipp, M., Tullis, J., Behrens, H., 2006. Effect of water on the dislocation creep microstructure and flow stress of quartz and implications for the recrystallized grain size piezometer. J. Geophys. Res.: Solid Earth 111 (B04201), 1–19.
Stipp, M., Tullis, J., Scherwath, M., Behrmann, J.H., 2010. A new perspective on paleopiezometry: dynamically recrystallized grain size distributions indicate mechanism changes. Geology 38, 759–762.
Stünitz, H., Thust, A., Heilbronner, R., Behrens, H., Kilian, R., Tarantola, A., Gerald, J.F., 2017. Water redistribution in experimentally deformed natural milky quartz single crystals—implications for H2O-weakening processes. J. Geophys. Res.: Solid Earth 122, 866–894.
Takahashi, M., Nagahama, H., Masuda, T., Fujimura, A., 1998. Fractal analysis of experimentally, dynamically recrystallized quartz grains and its possible application as a strain rate meter. J. Struct. Geol. 20, 269–275.
ter Heege, J.H., De Bresser, J.H.P., Spiers, C.J., 2005. Dynamic recrystallization of wet synthetic polycrystalline halite: dependence of grain size distribution on flow stress, temperature and strain. Tectonophysics 396, 35–57.
Tewari, V.C., 2012. Neoproterozoic Blaini glacial diamictite and Ediacaran Krol carbonate sedimentation in the lesser Himalaya, India. In: In: Bhat, G.M., Craig, J., Thurow, J.W., Thusu, B., Cozzi, A. (Eds.), 2012. Geology and Hydrocarbon Potential of Neoproterozoic–Cambrian Basins in Asia, vol. 366. Geological Society, London, Special Publications, pp. 265–276.
Thakur, V.C., Pandey, A.K., 2004. Late Quaternary tectonic evolution of Dun in fault bend/propagated fold system, Garhwal Sub-Himalaya. Curr. Sci. 87, 1567–1576.
Thakur, V.C., Pandey, A.K., Suresh, N., 2007a. Late Quaternary–Holocene evolution of dun structure and the Himalayan Frontal fault zone of the Garhwal sub-Himalaya, NW India. J. Asian Earth Sci. 29, 305–319.
Thakur, V.C., Pandey, A.K., Suresh, N., 2007b. Late quaternary–Holocene evolution of dun structure and the Himalayan frontal fault zone of the Garhwal sub-Himalaya, NW India. J. Asian Earth Sci. 29, 305–319.
Tokle, L., Hirth, G., Behr, W.M., 2019. Flow laws and fabric transitions in wet quartzite. Earth Planet. Sci. Lett. 505, 152–161.
Tsenn, M.C., Carter, N.L., 1987. Upper limits of power law creep of rocks. Tectonophysics 136, 1–26.
Tullis, J., Yund, R.A., 1985. Dynamic recrystallization of feldspar: a mechanism for ductile shear zone formation. Geology 13, 238–241.
Twiss, R.J., 1977. Theory and applicability of a recrystallized grain size paleopiezometer. Pure Appl. Geophys. 115 227 – 244.
Twiss, R.J., Moores, E.M., 2007. Structural Geology, second ed. Macmillan, pp. 736.
Verma, M., Bansal, B.K., 2013. Seismic hazard assessment and mitigation in India: an overview. Int. J. Earth Sci. 102, 1203–1218.
Warr, L.N., Cox, S., 2001. Clay mineral transformations and weakening mechanisms along the Alpine Fault, New Zealand. Geol. Soc. Lond. Spec. Publ. 186, 85–101.
White, S., 1977. Geological significance of recovery and recrystallization processes in quartz. Tectonophysics 39, 143–170.
White, S.H., 2010. Mylonites: lessons from eriboll. In: In: Law, R.D., Butler, R.W.H., Holdsworth, R.E., Krabbendam, M., Strachan, R.A. (Eds.), Continental Tectonics and Mountain Building: the Legacy of Peach and Horne, vol. 335. Geol. Soc. London Spec. Pub, pp. 505–542.
Whittington, A.G., Hofmeister, A.M., Nabelek, P.I., 2009. Temperature-dependent thermal diffusivity of the Earth's crust and implications for magmatism. Nature 458, 319.
Wiesmayr, G., Grasemann, B., 2002. Eohimalayan fold and thrust belt: implications for the geodynamic evolution of the NW-Himalaya (India). Tectonics 21. https://doi.org/10.1029/2002TC001363.
Wiltschko, D.V., Lambert, G.R., Lamb, W., 2009. Conditions during syntectonic vein formation in the footwall of the Absaroka Thrust Fault, Idaho–Wyoming–Utah fold and thrust belt. J. Struct. Geol. 31, 1039–1057.
Wojtal, S., Mitra, G., 1988. Nature of deformation in some fault rocks from Appalachian thrusts. Geol. Soc. Am. Spec. Pap. 222, 17–33.
Wolfowicz, A.M., 2012. Determining Temperatures of Deformation in Mylonites from the Scandinavian Caledonides, with Implications for the Thermal and Kinematic Evolution of Orogens. Boise State University Theses and Dissertations, pp. 607.
Xia, H., PlattJ, P., 2018. Quartz grain size evolution during dynamic recrystallization across a natural shear zone boundary. J. Struct. Geol. https://doi.org/10.1016/j.jsg.2018.01.007.
Yakymchuk, C., Godin, L., 2012. Coupled role of deformation and metamorphism in the construction of inverted metamorphic sequences: an example from far-northwest Nepal. J. Metamorph. Geol. 30, 513–535.
Yin, A., 2006. Cenozoic tectonic evolution of the Himalayan orogen as constrained by along-strike variation of structural geometry, exhumation history, and foreland sedimentation. Earth Sci. Rev. 76, 1–131.